HUMAN MASSETER MUSCLE STUDIES BY MAGNETIC RESONANCE

by

ERNEST W.N. LAM

B.Sc. (Hons.), The University of British Columbia, 1985
D.M.D., The University of British Columbia, 1989

A THESIS SUBMITTED IN PARTIAL FULFILMENT OF

THE REQUIREMENTS FOR THE DEGREE OF

MASTER OF SCIENCE

in

THE FACULTY OF GRADUATE STUDIES

(Department of Oral Biology)

We accept this thesis as conforming

to the required standard

THE UNIVERSITY OF BRITISH COLUMBIA

March, 1991

In presenting this thesis in partial fulfilment of the requirements for an advanced degree at the University of British Columbia, I agree that the Library shall make it freely available for reference and study. I further agree that permission for extensive copying of this thesis for scholarly purposes may be granted by the head of my department or by his or her representatives. It is understood that copying or publication of this thesis for financial gain shall not be allowed without my written permission.

Department of Oral Biology

The University of British Columbia
Vancouver, Canada

Date April 11, 1991

Abstract

The human masseter muscle is a structurally complex jaw elevator with the capability of generating high, multidirectional forces. The invasiveness of current anatomical and physiological methods has, however, limited both the number and scope of studies of human masseter muscle structure and function. Therefore the aim of this work was to apply *in vivo* magnetic resonance (MR) techniques to elucidate the three-dimensional internal architecture of the human masseter muscle and its metabolic response to exercise in order to gain a better understanding of the jaw muscles in health and disease.

In the first of these experiments, five adult subjects were selected and examined using cephalometric radiography, magnetic resonance imaging (MRI) and three-dimensional rotational and reconstructive computer graphics to describe the organization of tendon planes within the masseter muscle. Planar quadrilaterals representing putative tendon planes were fitted to the surfaces of the three-dimensional muscle reconstructions, and these were related to the mid-sagittal plane in the coronal and axial views. To confirm whether putative planes disclosed by MRI represented true anatomic entities, a fresh human cadaver head was imaged by MRI and then cryosectioned at millimetre intervals. Planar sections through the reconstructed muscle generated from the cadaver cryosections were correlated with the actual MR images in the same planes. Tendon plane angulation appeared to be related to ramal length and lower face height measured cephalometrically. In the axial view, the tendon planes appeared roughly to follow the angulations of the zygomatic arch and the lateral face of the mandibular ramus. Our results suggest that the angulation of tendon planes, and possibly pennation angles are different depending on the viewing angle, and infer that muscle fibres inserting on either side of a central tendon may need to develop different tensile forces if translation is to occur directly along the tendon axis.

In the second, ^{31}P magnetic resonance spectroscopy (MRS) was utilized to examine the masseter muscles of six adult males at rest and performing stereotyped isometric

clenching exercises. ^{31}P MR spectra were acquired from three locations within the muscle using a 2cm by 3cm, single-turn, copper receiver coil. The spectra were quantified on the basis of relative peak area and position. The organic phosphate (P_i) to creatine phosphate (PCr) ratio (P_i/PCr), which has been shown to be proportional to free ADP concentration and hence, the metabolic activity, as well as the normalized P_i concentration ([P_i]) and pH, were calculated for each site and exercise. The mean resting P_i/PCr ratio and [P_i] were greater for the deep part of the muscle than for the superficial and intermediate parts. These differences were significant to $p<0.01$. The mean pH however, was similar in all parts of the muscle at rest. During exercise, a significant increase in mean P_i/PCr was found in the superficial and intermediate parts of the muscle. Both these differences were significant to $p<0.05$. An accompanying decrease in mean pH was observed in all parts of the muscle during exercise. In the superficial part of the muscle, this decrease was significant to the $p<0.05$ level, and in the deep part, the decrease was significant to the $p<0.001$ level. No significant differences were found for these parameters between left and right molar clenching. These results suggest that metabolic activity may be monitored in the masseter muscle using ^{31}P MR spectroscopy and that task-dependent and regional variations in metabolic activity may be demonstrated both at rest and during exercise. They are promising enough to encourage future studies of muscle metabolism in subjects with jaw muscle disorders.

These experiments demonstrate the novel application of magnetic resonance techniques for studying craniomandibular morphology and function non-invasively. Collectively, they reveal the anatomical and functional heterogeneity which exist in the human masseter muscle.

Table of Contents

List of Tables

List of Figures

Acknowledgments

This work would not have been possible without the enthusiasm and support of Dr. Alan G. Hannam, *himself*, my research supervisor. I have learned a great deal from working with him as well as all the other members of my supervisory committee.

I am grateful to Ms. Joy Scott who, as Head Wrangler of the *HP9000/370* system, served as a valued link between myself and the computer, Mr. Bruce Sinclair who developed and implemented the novel surface rendering software which I came to know intimately, and Dr. Tom Korioth who gently introduced and guided me through the I-DEAS^{TM} package. I am also indebted to Dr. Ravi S. Menon who facilitated my introduction to the AHFMR *in vivo* NMR Facility at the University of Alberta in Edmonton, and Mssrs. Dan Gheorgiu and David Ellinger who designed and built the surface coil which was used there.

The University of British Columbia Dental Alumni Association generously funded a research endeavour at Loma Linda University where Dr. Ed Christiansen provided the knowledge and expertise to cryosection human cadaver heads. I was also fortunate to visit Drs. P. Baron and T. Debussy of the Faculté de Chirurgie Dentaire, l'Université de Paris, who showed me the masticatory muscles in yet another light, a trip which was made possible by Dr. G.S. Beagrie, then Dean of the Faculty. The Medical Research Council of Canada Farquharson Research Scholarships I held during the summers as an undergraduate freed me from some of the more mundane sorts of summer employment.

And finally, I am eternally grateful to my many colleagues who so generously gave of their time to act as subjects for my experiments.

CHAPTER 1

Introduction

1.0 Introduction to the thesis

Working independently, the research groups of Purcell (1946) and Bloch (1946) were the first to describe the response of nuclear magnetic dipoles in bulk matter to radiant energy. Since that time, nuclear magnetic resonance (NMR) has gained widespread use in solid state physics, physical and synthetic chemistry, and more recently, in biology, biochemistry and medicine, to answer a variety of questions relating to molecular structure and motion.

In more recent years, numerous technical advances in instrumentation have enhanced the sensitivity of NMR, enabling *in-vitro* as well as *in-vivo* investigations. The development of superconducting magnets brought improvements in magnetic field strength and homogeneity (Herfkens and Johnson, 1985), newer and more powerful computers made possible the use of more sophisticated data processing methodologies (Kumar et al, 1975) and spatial localization techniques not only allowed more accurate definitions of acquisition volumes, but contributed to improved signal-to-noise ratios and resolution (Ackerman et al, 1980). Among the first biological *in-vitro* studies was an investigation by Damadian (1971) which suggested differences in proton (^{1}H) relaxation characteristics between normal and cancerous tissue in the rat brain. Moon and Richards (1973) showed the feasibility of intracellular pH measurements in erythrocytes and shortly thereafter, Hoult et al (1974) obtained phosphorous (^{31}P) NMR spectra from in tact, excised rat hind limb muscle, demonstrating its potential as a monitor of metabolic activity and pH. However, in what was probably the most significant work of this period, Lauterbur (1973) described a method for spatially encoding the NMR signal, and mapped the distribution of a nuclear species. His experiments provided the basis for what is now magnetic resonance imaging (MRI).

Since its introduction nearly ten years ago into clinical medical radiology, magnetic resonance imaging has proven to be a unique methodology for the detection, localization and characterization of tissue, both normal and pathologic. MRI has been shown to be particularly effective in characterizing and determining the extent of disease in the central nervous, musculoskeletal and cardiovascular systems. *In vivo* magnetic resonance spectroscopy has, in comparison, gained slower acceptance in the radiologic community, despite the fact that important diagnostic information might be gained from examining the metabolic status of a particular organ system or lesion.

At present, the application of *in vivo* NMR techniques in clinical dentistry has been largely confined to investigations of the temporomandibular articulation. Until now, no applications have been made to other parts of the craniomandibular complex, for example, the jaw musculature, for which there is great potential value. The ability to assess both form and function non-invasively would be of particular benefit to researchers and clinicians alike.

The overall aim of this study was to expand the scope of NMR into other areas in the dental sciences. This was done through two separate, yet interrelated experiments involving structural and functional examinations of the human masseter muscle. The masseter muscle was chosen as a model for other multipennate jaw elevators because of its close association with jaw pathosis. Given the frequent occurance of hypertrophy, fatigue and pain in this muscle, the decision to use the masseter muscle as an experimental model is highly relevant.

Review of the Literature

1.1 Mammalian Masseter Muscle Architecture

Common to many mammalian jaw muscles is a system of internal aponeurotic or tendinous septa delineating discrete anatomically-distinct layers of muscle fibres with differing fibre orientations. In the human masseter muscle, three tendinous septa were

identified by Ebert (1939), and five sehnenspiegel were revealed from dissections performed by Schumacher (1961a). Both described these septa as extending into the muscle body from either the zygomatic arch, or the lateral surface of the mandibular ramus, with muscle attachments to bone (periosteum) or tendon. Illustrations within the text of Schumacher's (1961a) work showed the sehnenspiegel covering the complete antero-posterior dimension and upper or lower one-half to two-thirds of each muscle layer. Within each layer, the fibres were assumed to be arranged parallel to one another, and in some regions, they were depicted as being continuous between layers. In general, the organization of the muscle fibres displayed the classic multipennate arrangement described by Gans and Bock (1965).

Various anatomical criteria have been used to subdivide the human masseter muscle into smaller muscle subunits. DuBrul (1980) identified two incompletely separate portions of muscle within the human masseter muscle: superficial and deep. Ebert (1939) and McMinn et al (1981) each identified three overlapping layers of muscle, while Gaspard et al (1973) reported finding four *faisceaux*. Gaspard et al (1973) referred to these as masseter superficialis (lamina prima), masseter superficialis (lamina secunda), masseter intermedius and masseter profundus. Baron and Debussy (1979) also identified four elementary muscle *fascicles* in the human masseter muscle, first from gross dissection and then from areas or points of bony relief on five dry skulls. These they named masseter superificialis, laminae prima and secunda (F1), masseter intermedius (F2), masseter profundus, pars anterior (F3) and masseter profundus, pars posterior (F4). Irrespective of the number of muscle layers or divisions, both DuBrul (1980) and McMinn et al (1981) agreed that the muscle layers fused anteriorly and inserted together into the lateral aspect of the angle, ramus and coronoid process of the mandible.

A similar architectural arrangement was reported in the rat (*Rattus norvegicus* L.) masseter muscle by both Schumacher (1961b) and Hiiemae and Houston (1971). Schumacher's (1961b) dissections revealed a system of three sehnenspiegel, the most

superficial of which was thought to be a continuation of the temporal fascia (Hiiemae and Houston, 1971). Sehnenspiegel 2 was anchored to the mandibular ramus and extended into the inferior half of the muscle, while the deep sehnenspiegel 3 was located at the most medial aspect of the muscle. The rat masseter muscle has been variously described as consisting of from two (e.g. Romer, 1939 cited in Herring et al, 1979) to four (e.g. Becht, 1954 cited in Herring et al, 1979) discrete layers of muscle. In an attempt to reconcile this lack of descriptive uniformity, Hiiemae (1967) suggested that the separation of a muscle into parts where no anatomical division existed, might be justified when sufficiently marked differences in fibre orientation and position were present. On this basis Hiiemae and Houston (1971) chose to subdivide the rat masseter muscle into four parts: one superficial and three deep.

The canine (*Canis familiaris*) masseter muscle shares many of its internal characteristics with the human and rat masseter muscles (Schumacher, 1961c). Sehnenspiegel 1, anchored to the zygoma, covered over two-thirds of the masseter muscle, superficially. Beneath the first layer of muscle were three smaller, discontinuous, but closely apposed, tendon sheets (sehnenspiegel 2a, 2b, 2c) attached to the inferior border of the mandible. The remaining three sehnenspiegel were somewhat larger than these, but did not extend the full antero-posterior dimension of the muscle as in the masseter muscles of man, pig or rat. In the dog, however, more muscle fibres appeared to be anchored to periosteum.

In contrast, Herring and Scapino (1973) were unable to describe discrete, anatomically separate divisions in the masseter muscles of the ungulate pig (*Sus Scrofa* dom.). Schumacher (1961d) described four sehnenspiegel, two of which coursed almost the entire antero-posterior (dorso-ventral) dimension of the muscle. Small medial and lateral fingerlike projections were also depicted toward the anterior of the muscle. A bipennate fibre arrangement was shown in (Figure) Abb. 103b. in the sagittal view. These observations were consistent with the later work of Herring and Scapino (1973) who demonstrated a

complex three-dimensional arrangement of interdigitated, branched internal tendons in the muscle. A lateral aponeurotic sheet anchored to the zygomatic arch was termed the aponeurosis of origin. A major branch of this aponeurosis posteriorly, the medial aponeurosis, was described as running parallel and deep to the lateral aponeurosis, forming a pocket, open to the rear. Both the medial and lateral aponeuroses gave rise to minor branches paracoronally, forming small pockets for the muscle fibres in the deepest regions of the muscle. The aponeurosis of insertion, which was described as arising from the ventral edge of the mandibular angle, gave rise to muscle fibres originating from the aponeurosis of origin, and bone. Macroscopic examination of the pig masseter muscle (Herring et al, 1979) revealed gradual changes in fibre angulation dorso-ventrally at its surface. These observations lead Herring et al (1989) to the conclusion that it was not possible to identify strict anatomical compartments in muscle on the basis of fibre orientation alone since the angulation of fibres was not constant through the same muscle layer.

1.2 Mammalian Masseter Muscle Fibre Histochemistry

The human masseter muscle is heterogenous with respect to its fibre histochemistry. Muscle fibres have been characterized histochemically into three major groups which Bárány (1967) correlated with contraction velocity and fatigue resistance. Large diameter type I fibres were characterized by their slow contraction velocity, high oxidative capacity, and their high resistance to fatigue. Saltin (1973 cited in Hultman et al, 1981) suggested that type I fibres in limb muscles were recruited during low force activity. In the jaws, Taylor (1976) suggested that because type I fibres are engaged in more sustained contractile activity, they might be associated with parafunctional acts, such as tooth grinding. If contractile activity were sufficiently high, Taylor (1976) also suggested that type II fibres might be activated as well. During mastication however, when bite force is far below maximum, Ringqvist (1974) suggested the participation of type I fibres only. The distribution of type I fibres within the human masseter muscle as a whole has been reported variously as 28.6% (Ringqvist, 1974) and from 14% to 44% (Ringqvist et al, 1982). Eriksson and Thornell (1983) examined fibre

histochemistry within anatomically separate regions of the human masseter muscle and demonstrated type I fibres in between 61.6% and 71.8% of all fibres in all regions, except in the posterior superficial part, where they were more scarce (46.8%). In all sites, however, type I fibres comprised over 70% of the overall muscle fibre cross-sectional area, a finding qualitatively and quantitatively different from both limb and trunk muscles (Dubowitz and Brooke, 1973; Johnson et al, 1973; Häggmark and Thorstensson, 1979).

Smaller diameter type II fibres demonstrated faster contraction velocities (Edström and Kugelberg, 1968; Burke et al, 1973). Within the human masseter muscle, Ringqvist (1974) also demonstrated a positive correlation between maximum voluntary bite force and type II fibre size. Dubowitz and Brooke (1973) further subdivided type II fibres into IIA, IIB and IIC based on their staining activity. Type IIA fibres were reported to have high oxidative and glycolytic capacities, and therefore high fatigue resistance, while type IIB fibres demonstrated low oxidative capacity, but high glycolytic capacity, and were therefore deemed fatigue sensitive. The nature of the type IIC fibres remains uncertain, although several workers (Dubowitz and Brooke, 1973; Kugelberg, 1976; Jansson et al, 1978) have suggested a pluripotential role for them. In the human masseter muscle as a whole, type II fibre composition has been reported variously as 52.7% (Ringqvist, 1974) and between 37% and 79% (Ringqvist et al, 1982) of all fibres. Eriksson and Thornell (1983) found type IIB fibres present in between 19.3% and 25.5% in all biopsy sites, except the posterior superficial portion of the muscle, where they accounted for 43.1% of the total fibre population. In contrast, type IIA and IIC fibres were relatively rare. Ringqvist et al (1982) also reported the presence of intermediate staining, or IM fibres within the jaw muscles. Taylor (1976) postulated that these intermediate fibres belonged to the type IIC group because of their staining characteristics. Nonetheless, Ringqvist (1974) and Ringqvist et al (1982) reported these fibres to be present in 14.2% and between 7% and 19% of all fibres examined, respectively. Eriksson and Thornell (1983) reported smaller IM populations, with ranges of 3.2% and 8.2% in the five muscle regions. Together, these studies suggest that

the distribution of fibre types is not constrained by tendon boundaries and therefore not compartmentalized within the human masseter muscle.

In the rat masseter muscle, Hiiemae (1971) demonstrated a preponderance of pale staining muscle fibres in the superficial (81%) and two anterior deep portions (75% and 78%, respectively) of the muscle, and 59% in the deep masseter proper, suggestive of rapid and "phasic" mandibular movements. In another study (Suzuki, 1977) this fibre type was found in nearly 100% of all fibres examined, except in the deepest portion of the posterior part of the muscle. Similar fibre homogeneity was also demonstrated by Schiaffino (1974). In the canine masseter muscle, Suzuki (1977) demonstrated the presence of both fast- and slow-contracting fibres in a 4:1 ratio. These muscles appeared to be well adapted to powerful or sudden activity required for gnawing or biting, since they both had a high glycolytic capacity.

In the miniature pig, where mastication is both rapid and prolonged (Herring and Scapino, 1973), Suzuki (1977) also demonstrated a 3:1 ratio of fast- and slow-contractile units. These findings were later confirmed by Herring et al (1979), who found a large population (77%) of fast-twitch, oxidative fibres in the posterior portion of the muscle and 65% in the anterior part.

1.3 The Functional Basis of Muscle Pennation

An analysis of pennate muscle structure, such as the one outlined by Gans and Bock (1965) suggested that muscle fibres were anchored about a central tendon. When these fibres are activated, tension was developed at an angle α, the angle of pennation, to the tendon axis. This tension was resolved into two components, one which was oriented parallel to the tendon axis, and another which was aligned at right angles to this; the latter did not usefully contribute to the work of the muscle (Gans and Bock, 1965). The net result of this arrangement was displacement of the tendon plane and movement of the muscle as a

whole along the same axis when activated.

Numerous functional advantages have been proposed for muscle pennation (Gans and Bock, 1965). Of these, several are inappropriate for the externally situated masseter muscle, such as the ability to contract without an increase in diametric size, or to approximate parallel bony surfaces. Herring et al (1979) believed that compensation for muscle atrophy (Benninghoff and Ebinger, 1946; Benninghoff and Rollhäuser, 1952 cited in Gans and Bock, 1965) also seemed an unlikely explanation for muscle pennation. Recent work by Tanuma (1984) suggested increases in the lengths of terminal tendons accompanied by gradual muscle atrophy in masseter muscles from cadavers of increasing age. The remaining hypotheses emphasized either uniform or differential contraction of muscle parts.

The first of these suggested that the greater variety of muscle fibre lengths in pennate muscles allowed them to pack a greater number of fibres into a larger variety of spaces compared to parallel muscles. As well, far smaller bony areas were required for muscle attachment. While the increase in muscle fibre number might be expected to produce higher tensile forces, only those with pennation angles of 45° or less, were capable of producing the most useful forces. Therefore, pennate muscles may not necessarily be more efficient than parallel fibred muscles in this regard. It has also been suggested that pennate muscles may generate significantly longer excursions than parallel fibred muscles (Heinze, 1972 cited in Herring et al, 1979) because of their many different fibre angles, but experimental evidence by Herring (1975) demonstrated an inverse relationship between pennation and gape.

The second hypothesis suggested that selective contraction of fibre groups within the muscle would allow it to produce forces along more than one axis. Since the fibres in multipennate muscles were not all parallel, this might be a possibility (Gans and Bock, 1965).

A requirement for this would be an increase in the number of motor nerves as well as redistribution of motor efferents into specific regions of the muscle. Recent evidence from glycogen depletion experiments in the pig masseter muscle (Herring et al, 1989) suggested that motor units were sparsely distributed and randomly located throughout the muscle, most occupying between 5% and 20% of very small muscle volumes.

1.4 The Biochemistry of Skeletal Muscle Contraction

The energy of muscle contraction is derived from adenosine-5'-triphosphate (ATP) in a complex series of interactions in which the rate of energy usage is closely coupled to the rate of energy production. In skeletal muscle, the energy required for the mechanical work of muscle contraction is provided from the hydrolysis of ATP by actomyosin-ATPase:

$$ATP + H_2O \rightarrow ADP + P_i + \alpha H^+ + work$$

where the stoichiometry of H^+ (i.e. α) was calculated to be approximately 0.68 based on the dissociation constants of H_3PO_4 in acidic media (George and Rutman, 1960).

The mode of ATP biosynthesis is controlled by aerobic (oxidative) and anaerobic (glycolytic) pathways which are dependant on skeletal muscle fibre type. In prolonged, heavy exercise, aerobic oxidative phosphorylation is the primary mode of ATP synthesis in type I skeletal muscle fibres. A number of experimental models of oxidative metabolism (Hultman et al, 1981; Chance et al, 1985; Connett et al, 1990) have assumed a steady state relationship between ATP synthesis and breakdown, since this was considered to simulate the true physiologic condition (Chance et al, 1985). Of importance to the control of oxidative phosphorylation were 1) the rate of ADP and P_i delivery from cytosolic ATPases to the mitochondria, 2) the delivery rate of reducing equivalents in the form of NADH and 3) the partial pressure of oxygen (P_{O2}) in the circulation, although adjustments could be made in substrate concentrations to maintain a steady level of oxidative phosphorylation even with a falling P_{O2} (Chance et al, 1985; Connett et al, 1990). The overall biosynthetic reaction of ATP in the mitochondria by this pathway is:

$$3ADP + 3P_i + NADH + H^+ + \tfrac{1}{2}O_2 \rightleftharpoons 3ATP + NAD^+ + H_2O$$

If ATP is the primary energy source of muscle contraction, then creatine phosphate must be considered an important secondary source. Immediate resynthesis of ATP may be accomplished by cytosolic creatine kinase to restore ATP concentrations there.

$$PCr + ADP + aH^+ \rightleftharpoons ATP + Cr$$

ADP and P_i produced from spent energy are translocated across the mitochondrial membrane to activate oxidative phosphorylation there (Chance et al, 1986).

During active muscle contraction, ATP is consumed at a much higher rate that can be replenished by both the cytosolic creatine kinase and through oxidative phosphorylation. The biosynthesis of ATP through glycolytic pathways is an important mechanism of energy regeneration in contracting skeletal muscle, particularly in type II fibres. However, as the rate of ATPase activity approaches the maximum rate of oxidative phosphorylation in type I fibres, glycolysis begins to take over an increasing proportion of the metabolic burden. Classically, the explanation for this has been that part of the muscle is O_2 deficient and energy production must be supplemented by glycolysis. Recent work by Connett et al (1984, 1985) in the dog suggested that anaerobic glycolysis, even during low work intensities is critical for the production and maintenance of NADH for mitochondrial consumption and aerobic ATP production. At higher work loads, 50% of the energy utilized during voluntary work was derived from anaerobic glycolysis (Bergström et al, 1971).

Specifically, glycolysis refers to the anaerobic breakdown of carbohydrate, specifically glucose, to pyruvic acid. For each glucose unit entering the glycolytic pathway, two molecules (net) of ATP are generated (Kushmerick, 1983):

$$1glucose + 2ADP + 2P_i \rightarrow 2ATP + 2lactate$$

Ramaiah (1976) and Connett et al (1990) reported the control mechanism for

stimulating glycolysis during muscle contraction was achieved in an early step in the glycolytic pathway at the level of phosphofructokinase, through feedback inhibition of ATP and deinhibition by ADP, AMP and P_i. As ATP was utilized for energy, concurrent increases in ADP and AMP levels were observed. These metabolites stimulated phosphofructokinase activity as a direct result of decreases in concentration of the inhibitor and increases in the concentrations of the deinhibitors. Glycolysis increased, and ATP was synthesized at a higher rate to satisfy the demand (Newsholme and Start, 1973). However, the decrease in ATP concentration is matched with a far higher increase in ADP, so that ATP may not lead to sufficient stimulation of phosphofructokinase activity (Ramaiah, 1973), suggesting the importance of other factors.

Additional sites of enzyme-substrate inhibition have also been shown (Connett et al, 1990). The flux of ATP through the glycolytic pathway has been demonstrated to be dependant on the effect of P_i concentrations on the enzyme glycogen phosphorylase (Kushmerick, 1983). The activation of glycogen phosphorylase kinase in response to hormonal signals such as adrenaline (Issekutz, 1984) and insulin (özand and Narahara, 1984) has been shown in animal preparations to be of importance, as well as increases in intracellular Ca^{2+} (Newsholme, 1970) and alkalinization (Connett, 1987), the supply of glucose to the cell (Ahlborg and Felig, 1982) and the citric acid concentration (Connett et al, 1990).

1.5 Functional Heterogeneity within the Mammalian Masseter Muscle

There is little experimental evidence to support the notion of functional heterogeneity in the human masseter muscle. Using silver surface electrodes, Greenfield and Wyke (1956) measured simultaneous electromyographic (EMG) activity in the lower-anterior and upper-posterior portions of the masseter muscle during static intercuspal and unimolar contact, as well as during protrusive and retrusive acts. Their results showed the lower-anterior part of the muscle most active during intercuspal tooth contact, contralateral molar and incisor

biting, and during protrusion without tooth contact. The upper-posterior part of the muscle demonstrated the greatest activity during ipsilateral molar contact and jaw retrusion. They concluded that in addition to amplitude and frequency, the timing of electrical events should not be overlooked during electromyographic analysis. A fine-wire technique developed for measuring focal activity within the human masseter muscle was demonstrated by Belser and Hannam (1986) and Tonndorf et al (1989). Belser and Hannam (1986) showed differences in muscle activity between the deep and superficial portions of the masseter muscle, but during retrusive jaw clenching acts only. Unlike Greenfield and Wyke (1956), these workers were unable to demonstrate statistically significant differentiation of intramuscular EMG activity with different biting tasks.

Stålberg and Eriksson (1987) studied single motor unit topography in the human masseter muscle, and measured the medial-lateral extent of each territory. They demonstrated mean territories of 3.7±0.6 mm, with a range of 0.6 to 12.5 mm. In some regions of the muscle, longer scan lengths of up to 12.5 mm were reported through the entire muscle cross section. The positions of these recording sites within the muscle were, however, not identified. McMillan and Hannam (1989) argued that because the masseter is layered medial-laterally, the uniaxial, transverse trajectories used by Stålberg and Eriksson (1987) were clearly inappropriate. The experiments conducted by these workers made use of a stationary reference electrode and a roving probe a distance away. They demonstrated mean trajectories of 8.8±3.4 mm with a 5 to 20 mm range. The anterior-posterior dimensions of these territories were approximately double the superior-inferior and medial-lateral dimensions. Their findings implied that the sheet-like layers of muscle which make up the human masseter muscle were comprised of functional, cigar-shaped units.

Herring et al (1979) acquired simultaneous EMG data from multiple regions of the pig masseter muscle during mastication. Fine-wire bipolar electrodes were introduced into the superficial half of the anterior, middle and posterior regions of the muscle. Although

individual motor units were not detected, Herring et al (1979) demonstrated that parts of the muscle, not separated by tendon, were differentially active during the crushing, power and closing stages of mastication. This pattern was predominantly evident in the anterior-posterior dimension, and appeared as a wave of activity moving anteriorly during the masticatory cycle.

Heterogeneity of function was also demonstrated by Weijs and Dantuma (1975) in the rat masseter. Fine-wire electrodes were introduced into the four regions of the muscle previously described by Weijs (1973). They demonstrated that in general, the three deep parts of the muscle were active early in the preparatory stroke of mastication, with the superficial part becoming active in the late preparatory stroke and continuing until the end of the power stroke. Like Greenfield and Wyke (1956), Weijs and Dantuma (1975) also demonstrated temporal differences in activity, with peak EMG activity occurring at different times during the power stroke for the different muscle compartments.

1.6 Parafunctional Behaviour in the Jaws

Muscle contraction has been described as being either concentric, eccentric, or isometric (Christensen, 1985). Concentric and eccentric contractions are dynamic acts where there is a change of muscle fibre length with time. For example, when an object is lifted with elbow flexion, the biceps brachii muscle is said to be contracting concentrically. As the same object is lowered and the elbow is extended, the muscle is said to be contracting eccentrically. In contrast, isometric contraction is a static act, such as holding an object motionless at 90° elbow flexion. Biceps muscle fibres are held at constant length, and no external mechanical work is performed. Most tasks, however, are combinations of these with elements of dynamic as well as static components. For example, high velocity dynamic activity under a light load encompasses a small static component, but slow velocity dynamic activity incorporates a far larger static component.

Within the jaws, Christensen (1976) described eccentric contraction of the masseter muscle as laterotrusive movements of the jaw away from the intercuspal position (ICP), while concentric activity was described as corresponding to the return stroke of the teeth to ICP. During maximum voluntary tooth grinding activity, eccentric muscle contraction produced approximately one half of the electromyographic activity as concentric contraction on the working side. The amount of eccentric work was determined to a large extent by the amount of mandibular depression on the working side, cusp height and cusp angulation. The presence of balancing side contacts might also be of importance (Christensen and Mohamed, 1984; Shupe et al, 1984).

After dynamic jaw exercises, subjects reported feelings of weakness and instability up to twenty minutes after completion of the exercise under light load. Two to three hours later, weak to moderate deep pain was reported in the temporal regions, temporomandibular joints, peri-orbital regions, cheek and in the molar and premolar teeth. Pain was provoked by digital palpation as long as 20 hours later (Christensen, 1967) and lasted 2 to 3 days. Some pains were accompanied with sensations of muscle stiffness and swelling, fatigue and paraesthesia. While intramuscular tissue pressures were reported to be elevated (Christensen, 1971), no conclusive evidence was found for increased creatine kinase (Wallace et al, 1979; Cox and Rothwell, 1984) or mast cell activity (Christensen, 1978). As well, muscle biopsies showed no evidence of pathosis (Christensen, 1985). Blood flow, monitored using a ^{133}Xe clearance technique in the human temporalis muscle demonstrated an increase as high as 300% in intramuscular blood flow (IMBF) during tooth grinding (Bonde-Petersen et al, 1973) compared to resting values, the result of a post-exercise hyperaemia. Newham et al (1987) studied eccentric muscle contraction of the elbow flexors on three occasions, one week apart and demonstrated convincing evidence for muscle damage at the biochemical level. Their subjects reported the greatest muscle tenderness after the first exercise regimen. Plasma creatine kinase levels were elevated after the first exercise, but progressively decreased after the second and third regimens. In another study,

Newham et al (1983) reported that muscles which had contracted eccentrically showed histologically-evident fibre damage immediately after exercise, even though the magnitude of pain peaked 24 to 48 hours later. They suggested that while initial fibre damage is mechanically induced, the exacerbation of damage over time was due to mechanical or chemical factors.

Tooth clenching has been divided temporally, into three phases: fatigue, pain and tolerance (Christensen, 1985). This is an example of a static jaw exercise. EMG or bite force have typically been used in these studies to monitor maximum activity. The fatigue threshold, defined as the moment of appearance of an initial urge to stop isometric exercise because of a subjective sensation of slight discomfort or weakness at 100% of maximum voluntary clench (MVC) has been reported variously as 30sec (range, 15 to 60sec) in 20 to 40 year olds (Christensen, 1970, 1979, 1980a, 1981), and 50 to 60sec (range, 20 to 120sec) in 10 to 15 year olds (Christensen, 1980b). While these values appear not to vary significantly within individuals, there was significant variation between subjects. In both experiments, the sites of fatigue were typically reported within the masseter and anterior temporal muscles, although the feeling of numbness, lacrimation, perspiration and salivation were reported in the younger group. Pain threshold was reported around 55sec and pain tolerance at 118sec. Typically, immediate and total cessation of pain occurred between 2 and 5sec after completion of the activity. Studies of intra-muscular blood flow (IMBF) by ^{133}Xe clearance have also proven inconclusive in static jaw acts. Bonde-Petersen and Christensen (1973) demonstrated a 1.5 fold increase in IMBF during tooth clenching, but neither muscle EMG activity nor bite force were monitored. During biting at 22% to 37% maximum voluntary electrical activity (MVEA), monitored with bipolar surface electrodes positioned over the masseter muscles, and 45% to 55% maximum bite force (MBF), monitored with a force transducer at the first molar, no significant changes in IMBF were evident during clenching, although a marked post-exercise hyperaemia was reported (Rasmussen et al, 1983). Using two wire electrodes as monitors of superficial masseter

muscle activity, IMBF was measured at 50% MVEA by Monteiro and Kopp (1988). They demonstrated both elevations and depressions of individual IMBF, but on average a six fold increase in IMBF was observed during isometric contraction, and an eighteen fold increase was observed post-exercise.

1.7 Basic Principles of Nuclear Magnetic Resonance

The NMR phenomenon is complex and difficult to describe in terms of a single unifying set of processes. Therefore two discussions are presented, one based on quantum mechanical principles and the second on the more familiar theories of classical electromagnetism.

Certain nuclei which possess an odd number of protons and/or neutrons behave as magnetic dipoles, each of which is characterized by a magnetic moment μ, when placed into a static, external magnetic field B_o. The interaction of these magnetic moments and B_o gives rise to energy states which correspond to,

$$E = \mu \cdot B_o = \gamma_N (h/2\pi) I_z B_o$$

where γ_N is the gyromagnetic ratio, a characteristic of a particular nuclear species, h is Planck's constant and I_z is the spin angular momentum operator for the nuclear species. For hydrogen (^{1}H) and phosphorous (^{31}P) nuclei, the value of I_z is ½.

For spin ½ nuclei, two possible energy levels exist,

$$E(m_I) = \gamma_N (h/2\pi) m_I B_o$$

where m_I is the value of the spin angular momentum operator, operating on a nucleus. For spin ½ nuclei, the value of m_I is ±½ and the energy difference between them is given by,

$$\nu = (\gamma_N / 2\pi) B_o$$

in frequency units.

The number of nuclei in each of the two energy levels is determined by both

temperature, according, to the Boltzman distribution, and magnetic field strength (Bottomley et al, 1984). At room temperature, the excess of spins in the lower energy level results in a net magnetization M_o oriented parallel to B_o,

$$M_o = [N\gamma_N^2(h/2\pi)^2 I(I+1)]/3kT$$

where N is the number of nuclear spins at thermal equilibrium, k is Boltzman's constant and T is the temperature in degrees K. When RF energy of frequency v is applied to nuclei at their thermal equilibrium state, they are excited to the higher energy level.

In classical electromagnetic theory, a nucleus with magnetic moment μ can be likened to a spinning globe, precessing about a central axis at ω_o, the Larmor frequency.

$$\omega_o = \gamma_N B_o$$

In the Earth's magnetic field, the magnetic moments are randomly oriented. Under the influence of a static magnetic field B_o, the magnetic moments become aligned either parallel or antiparallel to this field. By convention, B_o is aligned along the +z axis. Those nuclei whose magnetic moments align parallel to the field are considered to be in the low energy spin state, while those aligned antiparallel are regarded as being in the high spin state. The net magnetization of the system M_o, is produced from a slight excess of nuclei in the low spin state.

Redirection of M_o is achieved with the application of an RF energy pulse in the form of a rotating electromagnetic field B_1, precessing with an angular frequency ω_1. This RF pulse can be regarded as an energy envelope of width $2/\tau_P$ (where τ_P is the pulse duration) which excites a range of frequencies. When $\omega_o = \omega_1$ the nuclei precess at the same frequency as B_1. Energy is absorbed by the system and M_o is redirected about an axis through an angle,

$$\theta = \gamma_N B_1 \tau_P$$

For example, a $\pi/4$ pulse applied about the x'-axis will drive the magnetization from its equilibrium state, 45° anticlockwise about the x'-axis. When B_1 is interrupted, the net

magnetization returns to its equilibrium state by two relaxation processes which occur simultaneously.

The first of these is termed T_1 relaxation. This process reflects energy exchange between nuclei and their surroundings, and is sometimes referred to as spin-lattice relaxation. The process is exponential in nature, and is governed by,

$$M_z = M_o(1-e^{-t/T1})$$

where M_z is the magnetization at time t. Tissue T_1s can be estimated using the expression

$$T_1 = A\nu^B$$

where A and B are tissue-dependent constants, and ν is the NMR frequency (Bottomley et al, 1984).

The second process T_2 relaxation results from the interaction of adjacent nuclear spins and produces spin dephasing. This is sometimes referred to as spin-spin relaxation. In a truly homogeneous magnetic field, T_2 relaxation is exponential in nature, and is governed by,

$$M_z = M_o e^{-t/T2}$$

In practice, however, small inhomogeneities in the magnetic field accelerate this process, and the signal decays after time T_2^*. Tissue T_2s are dependent on tissue type alone (Bottomley et al, 1984).

The NMR signal is received in the form of a free induction decay (FID). This is accomplished using a receiver coil tuned to the frequency of the NMR signal. The FID generates an electromotive force in the receiver coil and the variation of the NMR signal with time is transformed using a mathematical function called a Fourier transform (Kumar et al, 1975).

1.8 ^{1}H MR Biomedical Imaging

Image acquisition in MR imaging is achieved using a Fourier method first described by Kumar et al (1975) which relies on the application of linear magnetic field gradients of the kind first proposed by Lauterbur (1973). Magnetic field gradients are generated from three mutually perpendicular coil sets and each gradient produces a positional offset of the resonance frequency. For example, if a magnetic field gradient is applied in the z direction, G_z, then the resonance frequency becomes a function of the position, z. The acquisition process begins with the application of a slice select gradient in combination with an RF pulse. Therefore only spins with the Larmor frequency within the RF pulse frequency bandwidth are excited. Once a slice is selected, the slice select gradient is switched off, and signal encoding is then carried out along each of the two axes of the slice. At this time, all spins within the slice are precessing at the same frequency, and are said to be in phase. A read gradient, is then applied along one of the axes orthogonal to the first, causing the nuclei to precess at different frequencies depending on their positions along this axis. At the same time, a third gradient, orthogonal to the previous two, the phase encoding gradient, is applied, and its amplitude is incremented for each successive excitation, encoding positional data along the third axis. Typically, phase encoding gradients of different magnitudes are applied to acquire data from the 256 voxel rows which make up one side in the image.

RF pulses may be used to emphasize or de-emphasize differences in T_1 and/or T_2 relaxation between different tissues, thereby generating a means for image contrast. This is done by varying the manner in which the RF pulse(s) are applied. Tissue contrast in NMR imaging is dependent on the intrinsic T_1 and T_2 relaxation times, and proton density for each tissue. Tissue contrast based on differences in ^{1}H density may be achieved by choosing a relatively long repetition time (T_R) compared to T_1, so that T_1 will have little impact on contrast, and a relatively short T_E so that T_2 contributions will be minimized. A T_2 weighted image can be obtained by choosing $T_R \gg T_1$, so that T_1 contributions are minimized. As T_2 does not vary with magnetic field strength, contrast related to T2 differences are

maintained. As T_1 does change with magnetic field strength, T_R must be carefully chosen to maximize contrast. At 0.15T, skeletal muscle T_1 and T_2 measurements have been reported to be 250ms±20% and 50ms±20%, respectively and for adipose tissue, this has been calculated to be 170ms±20% and 80ms±20% (Young et al, 1986). King et al (1984) utilized a spin-echo (SE800/60) sequence to study the human knee and found that the short T_R and long T_E were ideally suited for visualizing morphological details of the normal adult knee. They found that this combination of T_R and T_E provided the greatest grey-scale contrast between tendon, muscle and fat.

The most commonly applied pulse sequence in musculoskeletal MRI has been the spin-echo (SE) sequence. A $\pi/2$ pulse is first applied about the x'-axis in the rotating frame, tipping the magnetization, M_o, into the x'-y' plane along the +y'-axis. The nuclear spins then begin to dephase by T_2 relaxation, with some spins continuing to precess faster than $_o$ and others slower, and by T_1 relaxation. A π pulse applied after some time T_E, the echo time, about the x'-axis has the effect of rotating the spins 180° about x', refocussing the spins along the -y'-axis (this is the "echo"). The time between successive applications of the ($\pi/2$-T_E-π-Acquire) sequence is the repetition time (T_R).

Unger (1985) used a 1.3T magnet, and 5mm and 10mm sagittal and coronal images to evaluate normal human orofacial anatomy with MRI. While hers was a preliminary investigation of normal anatomy, her initial opinion was guarded for imaging the oral cavity. Seltzer and Wang (1987) attempted to depict normal anatomy and pathosis in the human masseter muscle, but showed only one MR image of the normal muscle. Schellhas (1989), in a retrospective study of some 4000 MRI studies of the temporomandibular joints, head, brain, salivary glands and orofacial region reported on incidental findings of pathosis in the masticatory muscles. Throughout the work however, the deep temporal muscle is consistently mislabelled as the medial pterygoid muscle, although it extended as far superiorly as the attachment site of the superior head of the lateral pterygoid muscle. He

also attempted to demonstrate "torn" muscle fibres despite the limits of the instrument's resolution.

The cross-sectional area of whole human masseter muscles has also been measured and its angulation determined in three-dimensional space (van Spronsen et al, 1987; Hannam and Wood, 1989; Koolstra et al, 1990) for biomechanical measurements.

1.9 ^{31}P MR Spectroscopy of Skeletal Muscle

Recently, *in-vivo* ^{31}P nuclear magnetic resonance spectroscopy has been used to study cellular metabolites in normal (Taylor et al, 1983; Chance et al, 1986; Helpern et al, 1989) and diseased (Hands et al, 1986; McCully et al, 1988) human muscle, non-invasively.

The ^{31}P NMR spectrum typically displays seven resonance peaks of varying line width and intensity across the sampled frequency range, corresponding to phosphomonoester (PME), which consist of praecursors of membrane biosynthesis, and sugar phosphates, inorganic, cytoplasmic phosphate (P_i), phosphodiester (PDE), which consist of the hexose phosphates, creatine phosphate (PCr) and γ-, α- and β-ATP (Hoult et al, 1974; Bailey et al, 1981; Chance et al, 1986). The ^{31}P signal was not found in human skin or fat, while phosphate in bone was considered too anisotropic to yield a sharp signal (Taylor et al, 1983).

The ^{31}P NMR spectrum is much simpler to interpret than the equivalent ^{1}H spectrum because phosphorous nuclei appear in a smaller number of chemical environments. Magnetic shielding from adjacent bonding electrons and the magnetic effect of other nuclei vary the resonance frequency of individual nuclei over a small range. The chemical shift δ, is a measure of this variation and is reported in units of ppm relative to the position of an internal standard. In ^{31}P NMR, this is typically the PCr peak.

$$\delta = [(\nu - \nu_r)/\nu_r]10^6$$

where ν and ν_r are the resonance frequencies of a chemical species of interest and the reference species, respectively.

Validation of the NMR-derived concentrations of P_i, PCr and ATP, as well as pH, were carried out in several different animal muscles including cat soleus and biceps muscles (Meyer et al, 1982), northern frog gastrocnemius muscle, toad gastrocnemius and chicken pectoralis muscle (Burt et al, 1976). Both groups found excellent agreement between NMR-derived values and those found using the more traditional freeze-clamping methods. Taylor et al (1983) also found excellent agreement between NMR-derived intracellular pH measurements and those obtained from tissue homogenates. Roos and Boron (1981) considered the ^{31}P NMR method of determining pH to be superior to conventional methods. In most NMR-determinations of P_i concentration, it is often found to be substantially less than that which is obtained using the freeze-clamping method of extraction. Meyer et al (1982) have observed that this appeared to be more of a problem for fast twitch muscles. Two possible explanations have been proposed for this. The first of these suggested that during freezing and extraction of the metabolites, there was an artifactual hydrolysis of PCr. The second explanation suggested that a significant proportion of P_i existed in a bound state in the mitochondria which, while not detectable by NMR methods, was liberated during the extraction process.

Absolute metabolite concentrations, proportional to peak areas, have been calculated, but assume a standard concentration for one metabolite (ATP) at the outset of calculation (Taylor et al, 1983; Meyer et al, 1985; Hands et al, 1986). More useful, have been ratios the peak areas, provided the effects of partial signal saturation are addressed (Taylor et al, 1983). The P_i/PCr ratio has been shown to be proportional to the free ADP concentration and has been used as a measure of metabolic activity within the muscle. This has been reported variously as 0.10 in human flexor digitorum profundus muscle (extracted from Taylor et al, 1983), 0.12±0.01 in the human wrist flexor muscles (McCully et al, 1988),

and 0.14±0.03 in human gastrocnemius muscle (McCully et al, 1988). McCully et al (1989) found no difference in the resting P_i/PCr ratio of trained versus untrained individuals.

In an attempt to relate muscle fibre type to this parameter, Meyer et al (1985) studied slow- and fast-twitch muscles in the cat hind limb. They demonstrated mean resting P_i/PCr ratios of 0.089 in cat biceps muscle which is composed of greater than 75% fast-twitch, glycolytic fibres, and 0.568 in cat soleus, which is greater than 92% slow-twitch, oxidative fibres. They suggested that differences in these ratios between different muscles and within regions of the same muscle might prove useful for routine non-invasive estimation of fibre type in humans.

During steady state dynamic exercise, McCully et al (1989) reported an increase in the P_i/PCr ratio to 1.36±0.14 and 1.32±0.13 for trained and untrained individuals, respectively in the human wrist flexor muscles. McCully et al (1988) did not observe changes in this ratio during isometric exercise. Taylor et al (1983), however, reported changes in the PCr/(PCr+P_i) ratio in flexor carpi radialis following a non-lengthening, exercise protocol, with 90% metabolite recovery within 5 minutes. Cady et al (1989) found no significant differences in any of the metabolite levels during isometric exercise at 50% and 100% of maximum. Elevations in the P_i/PCr ratio have also been observed in subjects with neuromuscular disease associated with muscle fibre damage. This has lead McCully et al (1988) to conclude that changes in the P_i/PCr ratio reflect non-specific muscle damage in normal and diseased subjects. Cohen et al (1989) examined whole human masseter muscles using ^{31}P NMR spectroscopy and demonstrated that subjects diagnosed as myofacial pain dysfunction syndrome patients displayed a less evident phosphate ratio signature and that they were unable to recover as quickly to a rest "signature" value compared to asymptomatic subjects.

The chemical shift between the P_i and the PCr peaks has been used as an indicator

of intramuscular pH (Hoult et al, 1974; Dawson et al, 1977; Gadian et al, 1979). The PCr peak has a relatively low pK_a (4.6) and hence is insensitive to pH changes near neutrality (Challiss et al, 1988). In contrast, inorganic phosphate, which exists as two species in solution, HPO_4^{2-} and HPO_4^{-}, is quite sensitive to pH changes (pK_a=6.8) near physiologic pH (Meyer et al, 1985). These species exchange at a rate of between 10^{-9} to 10^{-10} s^{-1}, but in the absence of exchange, the two peaks would be separated by 2.3 ppm. Chance et al (1986) have reported that while peak position may be measurable to an accuracy of 0.02 ppm, an error of up to 0.1 pH units may occur for pH calculations. The resting pH in human skeletal muscle derived from ^{31}P NMR spectra has been reported to be 7.03±0.03 in human flexor digitorum superficialis (Taylor et al, 1983), 7.02±0.02 and 6.98±0.02 in trained and untrained human wrist flexor muscles (McCully et al, 1989) and 7.10±0.03 in human first dorsal interosseous muscle (Cady and Newham, 1989) during steady state exercise. Meyer et al (1985) found a resting pH of 7.18 in both fast- and slow-twitch muscles of the cat hind limb. During dynamic exercise, Taylor et al (1983) reported a mean decrease in pH to 6.4 and 6.8 in the human finger and wrist flexors, respectively. McCully et al (1989) reported a decrease to 6.87±0.089 in untrained subjects. Cady and Newham (1989) reported a pH drop in human first dorsal interosseous muscle during isometric exercise to 6.60±0.11 and 6.61±0.09 at 50% and 100% maximum voluntary contraction. McCully et al (1989) reported that trained subjects in ramp exercise tests had a significantly higher ($p<0.05$) end-exercise pH (6.91±0.04) compared to untrained subjects (6.72±0.07).

It has been acknowledged that one of the difficulties in studying metabolic activity in muscle is that of tissue heterogeneity (Busby et al, 1973; Taylor et al, 1983; Park et al, 1987; Challis et al, 1988; McCully et al, 1989). Asymmetric broadening or splitting of the P_i resonance is believed to be an indication of pH heterogeneity within the muscle (Taylor et al, 1983; Park et al, 1987). Taylor et al (1983) interpreted this finding as signal from an inactive second muscle, present within the acquisition range of the receiver coil due to poor localization techniques. In contrast, Park et al (1987) attributed this splitting to the presence

of two functional pools of fibres within the same muscle. They observed split P_i peaks in only 4 of 10 untrained individuals, however, following three grades of exercise and recovery, in the wrist flexor muscles. In an attempt to resolve this ambiguity, Jenesson et al (1989) used 6cm and 2.3cm diameter surface coils and found peak splitting with the 6cm coil only. They concluded that although the contribution of different fibre types should not be excluded, the interpretation of the peak splitting, based on a method which could not guarantee localization of one muscle can prove hazardous. Challis et al (1988) disclosed differences in [PCr] and pH through four 3mm to 4mm slices through the rat vastus lateralis muscle. They demonstrated a [PCr] decrease from 0.95±0.01 to 0.88±0.01 from the superficial layer to the deep layer, as well as an increase in pH from 7.01±0.02 to 7.08±0.03, for the same progression. During steady state stimulation, these values decreased to 0.60±0.02 to 0.70±0.02 and 6.99±0.02 to 7.04±0.01, respectively.

CHAPTER 2

Statement of the Problem

The multipennate human masseter muscle is both structurally and functionally complex. Under normal operational conditions, the human masseter muscle has been shown to be functionally heterogeneous, but the relationship between structure and function remains vague.

In the past, anatomical and behaviourial studies of muscle in both the limbs and jaws have been highly invasive. Anatomical investigations of muscle structure have relied on gross and histological sectioning of cadaver material, despite the fact that the dispositions of living tissues may be different to those fixed by preserving solutions. This makes three-dimensional quantification of structure difficult, unless judicious measures are taken to maintain the integrity of the muscle. This is particularly important in the case of multipennate muscles in which the arrangement and disposition of tendon and fascia within the muscle serve as attachment sites for muscle fibres, and provide conduits for nerves and vessels. Changes induced in these intramuscular connective tissues as a result of excessive muscle tension may have pathological ramification, but cannot be explained without an appreciation of regional intramuscular biomechanics. This, in turn, depends upon an understanding of regional morphology.

Functional studies of muscle have relied on intra-muscular fine-wire and needle electrodes to measure muscle electromyographic activity. Radioactive isotopes have been employed to monitor intra-muscular blood flow, and the direct excision of muscle biopsy specimens has been utilized to examine metabolic activity. Wire and needle recordings of muscle activity are, however, highly focal and measure electrical events only, and the results of intramuscular blood flow measurements so far have been ambiguous. Studies of metabolic activity in in tact muscles would allow further insight into muscle function in both

normal subjects and patients, but these studies have been limited in the case of the human jaw muscles.

The overall goal of the present work was to apply NMR to the study of structure and function in the jaw muscles in living subjects. Two hypotheses were posed:

1. That intramuscular, structural features in the human masseter muscle can be revealed and measured in three-dimensions by ^{1}H magnetic resonance imaging. This hypothesis was tested utilizing cryogenic sectioning of a fresh cadaver masseter muscle, cephalometry, magnetic resonance imaging and three-dimensional rotational and reconstructive computer graphics.

2. That metabolic activity and pH in the human masseter muscle vary regionally according to task, and can be measured by means of ^{31}P magnetic resonance spectroscopy. This hypothesis was tested using a bite force sensing device and ^{31}P magnetic resonance spectroscopy.

CHAPTER 3

Materials and Methods

3.1 Three-Dimensional Computer Reconstruction of Tendon Planes in Human Masseter Muscle

In order to describe the disposition of tendon and muscle tissue within the human masseter muscle, a human cadaver head, less than 24 hours post-mortem, was embedded in high density polyurethane foam within a 12ins diameter section of plastic pipe. This was then scanned using a GE8800 CT system (General Electric Medical Systems, New Berlin, WISC.) to determine the precise orientation of the specimen within the polyurethane. Cryogenic sectioning of the specimen was performed at 1.0mm intervals using a 20ins jointer saw. Photographs were then made of each freshly milled surface. The specimen was kept frozen by immersion in a slurry of dry ice and 200 proof punctilious ethanol (-78.5°C) between sectioning (Christiansen et al, 1987) (Figure 4.4A)

Tendon and muscle outlines were traced directly from photographic slides of the cadaver muscle and digitized using an HP9000/375 computer system and peripherals (Hewlett-Packard Ltd., Palo Alto, CA.) with a resolution of one point per 0.3mm on the original tracing. From these data, 50 points were selected to describe the boundary of each tissue section. All data were numerically coded and arranged within a common three-dimensional coordinate system (Hannam and Wood, 1989). Graphics software (I-DEAS^{TM}, Structural Design Research Corporation, Milford, OH.) permitted retrieval of individual sections, their assembly and graphical representation in three-dimensions.

3.2 Estimation of Tendon Plane Orientation within Human Masseter Muscle from Reconstructed Magnetic Resonance Images

Five fully dentate adults between the ages of 23 and 39 were selected at random for the study on the basis of craniofacial type and malocclusion. These included 3 males and 2

females.

3.2.1 Cephalometry

It was expected that overall differences in craniofacial type might affect the disposition of tendon planes within the respective muscles. In order to specify the craniofacial dimensions of each subject, lateral cephalometric radiographs were obtained using a Model W105 Counterbalanced Cephalometer (Picker, Cleveland Park, OH.). In each case, a 165cm source-to-subject distance was used, a 14cm subject-to-film distance and 1.25sec exposures were made at 90kVp and 15mA. From these, selected angular and linear cephalometric variables were measured according to criteria and definitions by Lowe (1980) and Weijs and Hillen (1986). The anterior position of the maxilla was defined by the angle SNA, the anterior position of the mandible by the angle SNB and relative mandibular prognathism by the angle ANB. Cranial base angle was defined by BaSN, gonial angle as ArGoMe, palatal plane angle as (ANS)(PNS)SN and mandibular plane angle as SNGoMe. Ramal height was measured as the linear distance ArGo, mandibular length as GoPg, upper face height as the linear distance Na(ANS), lower face height as (ANS)Me and anterior cranial base length as SN. In addition, bizygomatic and bigonial widths were measured directly from each subject at the zygomatico-temporal suture using a Denar (Denar Corp., Anaheim, CA.) facebow. One half the difference of these two measurements has been used as an estimate of masseteric width (Brown, 1973).

3.2.2 Validation of the Approach

To confirm the conformity of muscle tissue and tendon from the MR images with the actual morphology, a human cadaver head (see 3.1) was imaged utilizing a SE500/17 sequence with 4 signal averages at 1.0T with a Siemens Magnetom imaging system (Siemens Medical Systems, Iselin, N.J.). One-twenty (120) format colour slides of the coronal cryosectioned muscle and the MR images were then compared visually under magnification. In addition, computer-generated planar cuts of the masseter muscle

reconstruction (generated in 3.1) were compared with the MR images in the same planes.

3.2.3 Magnetic Resonance Imaging of Subjects

Magnetic resonance imaging was performed on a Picker Vista MR 1100 system (Picker International, Wembley, England), operating at 0.15T. Each subject was asked to lie in a supine position on the unit's gantry bed. Before being placed in the magnet, the subject's head was aligned with the aid of a laser-light referencing system so that the Frankfort horizontal plane was perpendicular to the plane of the gantry bed. A 10cm diameter, customized two-turn copper surface coil was then positioned over the right masseter muscle of each subject, and the centre of the static magnetic field was referenced through the centre of the coil. During imaging, each subject was asked to bite lightly into the intercuspal position. With the goal of generating the best MR image contrast between adipose tissue, muscle and tendon, two spin echo (SE) sequences were employed, the first utilizing a 26msec echo time (T_E) and the second using a 60msec T_E, and an 833msec repetition time (T_R). Using this pulse sequence, adipose tissue produced the highest intensity signal. In contrast, cortical bone was a weak signal-producing tissue and was seen as a black outline surrounding the cancellous bone of the mandible. Teeth were also weak signal-producing entities and appeared black. Muscle was intermediate in intensity between adipose tissue and cortical bone. Muscle tissue was slightly more signal intense with the 26msec T_E than with the 60msec. Images using an inversion recovery (IR) sequence were obtained with a 125msec inversion time (T_I) and a 2000msec T_R. Using this pulse sequence, adipose tissue had low signal intensity, while muscle and tendon appeared similar to the spin echo images. A free induction decay (FID) using a 400msec T_R generated images of muscle and adipose tissue in which the intensity of both tissues was equally strong. The spin echo sequence utilizing an 833msec T_R, a 60msec T_E and four signal averages was ultimately chosen for image generation.

As the circular coil allowed only image acquisition unilaterally, a bilateral two-turn

surface coil was built using Tygon-covered 3/8ins diameter copper tubing. The coil was then tuned to the appropriate proton frequency at 0.15T. At maximum signal attenuation (30dB) a satisfactory image could not be generated without overloading the capacity of the receiver coil. Therefore, a second prototype bilateral, single-turn coil was built and tuned in a similar manner. The design of the bilateral coils prohibited changes in width to accommodate different facial widths. Therefore, for narrow faces, image signal-to-noise was compromised because the coil was not closely apposed to the face. The circular coil was chosen despite its shortcomings.

As image quality is dependent on slice thickness, 5mm contiguous MR sections through the masseter muscle in the sagittal plane generated four, possibly five images of the muscle. Varying the position of the excitatory RF pulse through the muscle enabled selective excitation of different 5mm volumes. By offsetting the acquisition volume of successive 5mm slice sets, it was possible to generate images through slightly different volumes of the muscle. Initially, a series of 10 contiguous 5mm slices was obtained in the sagittal plane of section. A second series was then obtained in the same plane with a 2mm offset with respect to the first. A third and final series was obtained in a similar manner. The result was a series of 30 contiguous and overlapping sections through the muscle.

To test the validity of this approach in image reconstruction, a phantom was constructed which was comprised of a lucite box containing a 1cm diameter acrylic bead and an extracted human mandibular incisor tooth. The phantom was imaged using the SE833/60 sequence described earlier to obtain images through both the bead and the tooth simultaneously. Zero, 1, 2, 3 and 4mm slice offsets were used to generate a series of 10 overlapping images with 1mm steps through the bead and tooth. The images were then traced, digitized and formatted using custom-designed computer software to reconstruct the two objects in three-dimensions.

To resolve optimally the internal architecture of the masseter muscle, coronal sectioning was chosen. Because of the proximity of the deep compartment of the muscle to the temporalis muscle, and signal averaging, axial sectioning would not permit this division to be visualized. Signal averaging would also hinder visualization of tendon planes in the sagittal plane. An evaluation of magnetic field homogeneity and spatial resolution of the instrument revealed that consistent quantitative measurements could be made in a 12100 cm^3 volume at the centre of the magnet with 1mm spatial resolution (Stewart, 1986).

In order to examine the effect of the slice thickness on image quality, one subject was imaged using a Philips Gyroscan 1.5T S15/High Performance superconducting system (Philips Medical Systems, Shelton CT.). A SE500/30 sequence with 4 signal acquisitions was used to obtain a series of contiguous, sagittal 5mm sections. A second image set was obtained in a similar manner with 3mm sections and a 2mm gap between slices. These sets were then compared visually under magnification. While image signal-to-noise was expectedly poorer for the 3mm slices, the only other difference between the two was that tissue borders were not as well defined in the 3mm set compared to the 5mm set.

3.2.4 Muscle Breadth Measurements

The breadth of each muscle compartment was measured in the coronal view. This was accomplished by locating the midpoint of a line connecting the superior- and interior-most points of each compartment. A measurement was then made perpendicular to this line. This was done for all compartments on each MR image. As the tendon planes partition the muscle obliquely, it would appear that the angulation of the tendon planes would be affected most by changes of muscle breadth along this axis, rather than the one parallel to the Frankfort plane.

3.2.5 Three-dimensional Computer Reconstructions and Tendon Plane Angle Estimation

Tracings of muscle boundaries on the MR images were digitized using an HP

9000/375 computer system and peripherals (Hewlett-Packard Ltd., Palo Alto, CA.) capable of 0.3mm point-to-point resolution (Figure 4.4C). From these data, 50 points were selected to describe the boundary of each muscle section (Figure 3.1). Tendon planes were clearly visible within the intramuscular and connective tissue voids left by tendon in each muscle reconstruction, corresponding to the regions described by Ebert (1939) and Schumacher (1961a). Putative tendon planes were defined by aligning software-controlled planar quadrilaterals within these voids, and were described mathematically as unit vectors perpendicular to the chosen planes in three-dimensional space. Planar angulations were expressed relative to the mid-sagittal plane, defined as the unit vector [1,0,0] and to the coronal plane, defined as [0,0,1]. This method overcame the uncertainty of identifying the same object in three mutually orthogonal planes. It was reproducible to within 3.1° in any one plane as determined from ten sequential mathematical fits made to the same structural outline.

Figure 3.1 Line tracing of a complex masseter muscle contour (a) and its graphical representation by 50 data points (b).

b

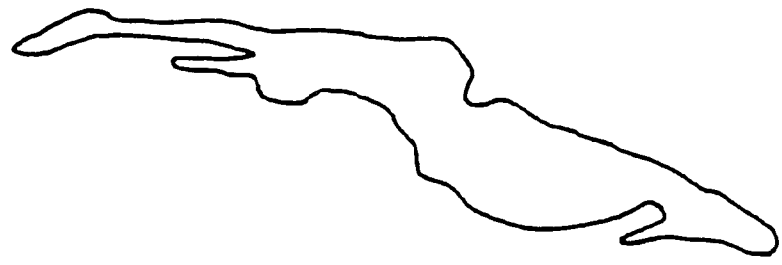

a

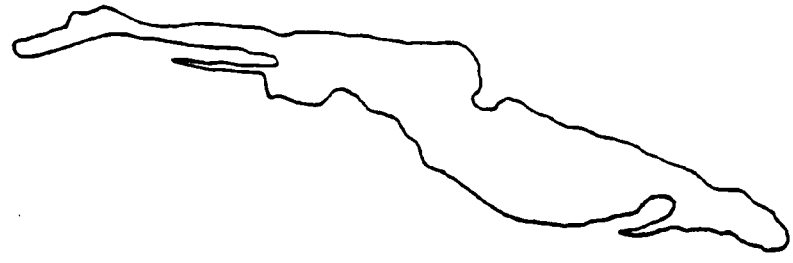

3.3 Regional ^{31}P Magnetic Resonance Spectroscopy of Exercising Human Masseter Muscle

Six fully dentate adult male subjects between the ages of 26 and 33 were selected for this part of the study. Informed consent was given by all subjects and approval for human experimentation was granted by the Ethics Committee of The University of British Columbia.

3.3.1 Bite Force Transducer and Occlusal Stop Fabrication

Study casts were obtained for each subject and mounted on a Denar Mark II semi-adjustable articulator (Denar Corporation, Anaheim, CA.). These were used to construct a novel bite force monitor which could be inserted between the teeth with minimum jaw separation. The device incorporated a force sensing resistor (FSR^{TM}, Interlink Electronics, Santa Barbara, CA.), which changed resistance in a predictable manner with the application of force to its surface. The electrically active material consisted of a variety of metallic-type conductors and semi-conductors, as well as surface conductive components, imprinted onto a tough polymer film with a thickness which did not exceed 0.8mm. Each FSR^{TM} was calibrated for static loads by means of an MTS-T 5002 tensile testing machine (Machine Testing Systems, Southamptom, England). A steel dome, approximately the shape of a thumb tack head, was lined with cold-cure acrylic resin (Duralay, Reliance Dental Manufacturing Co., Worth, ILL.) and bonded to one surface of the FSR^{TM} provided the load point during calibration. The FSR^{TM} was then incorporated in a flat acrylic resin shim to the occlusal surface of the mandibular right first molar tooth (Healthco Inc., Dental Division, Boston, MASS.) (Figure 3.2). Opposing this was a flat, metal wafer, adapted in a similar manner to fit the surfaces of the opposing maxillary dentition, so that the forces generated at the interface between the flat metal plane and the dome would be distributed evenly to the sensing surface of the FSR^{TM} (Figure 3.2). Inter-incisor separation did not exceed 4.5mm.

During the MR session, each subject clenched on a matching interocclusal stop constructed from cold-cure acrylic resin which conformed to the mandibular left and right

first molar teeth (Figure 3.3). Each stop was approximately 4.5mm in thickness, measured at the at the incisors with the articulator opened vertically from the subject's intercuspal position.

3.3.2 Calibration of the Force Transducer

The ½" diameter circular FSR^{TM} provided consistent results for forces over 100N. For loads less than this, the device was inconsistent. An example of a calibration curve for an FSR^{TM} used by one of the subjects is shown in Figure 3.4. The calibration curve is linear when plotted as log V vs. log F ($r=0.988$), where V represents the output signal in volts and F represents the applied force in Newtons.

3.3.3 Exercise Protocol

While the non-ferrous FSR^{TM} was ideal for use near high magnetic fields, a recording system could not be constructed which did not require an externally placed circuit. It was found that the copper lead, which linked the FSR^{TM} to the amplifying circuit, although non-ferrous, acted as a secondary radiofrequency (RF) antenna and interfered with the primary antenna, which was the surface coil. Before the experiment, each subject was trained in a stereotyped exercise protocol (1sec clench, 1sec rest) for 256sec, the time estimated for nuclear magnetic resonance spectroscopy. While each subject demonstrated different mean bite forces ranging between 272N to 479N, each was able to maintain steady, near-maximal, intermittent clenches for the duration of the exercise period. To ensure that each subject maintained pre-trial force levels, right sided bite force was recorded immediately after MR spectroscopy. Pre- and post-exercise peak bite force measurements were obtained at 20sec intervals during the exercise protocol and plotted against time (Figure 3.5).

Figure 3.2 Bite Force Monitor Cold cure acrylic resin-lined FSR^{TM} and steel dome adapted to mandibular first molar tooth and cold cure acrylic resin-lined metal wafer adapted to opposing maxillary dentition.

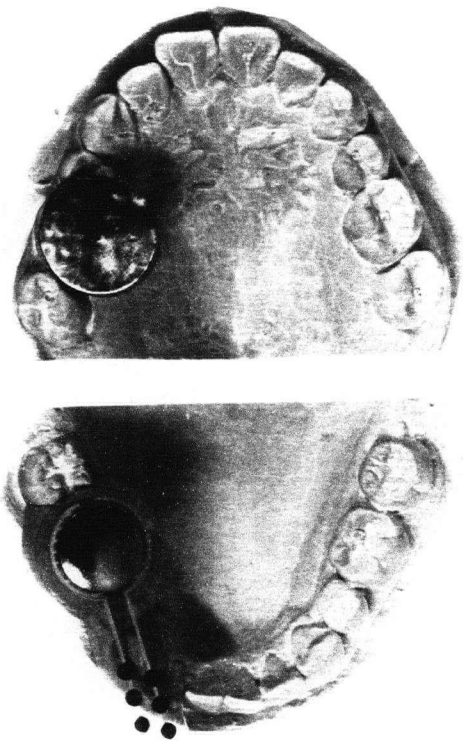

Figure 3.3 Occlusal Stop fabricated for one subject.

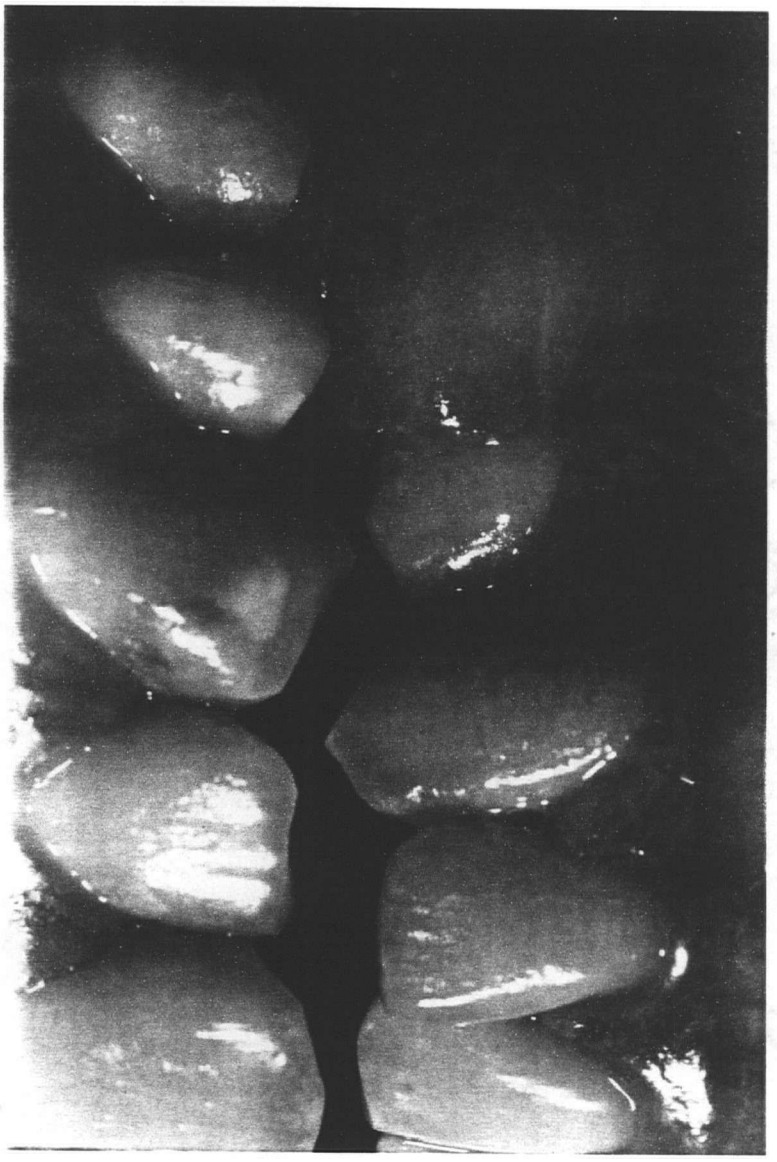

Figure 3.4 Calibration curve of an FSR^{TM} where V represents the output signal in Volts and F is the bite force output in Newtons (N).

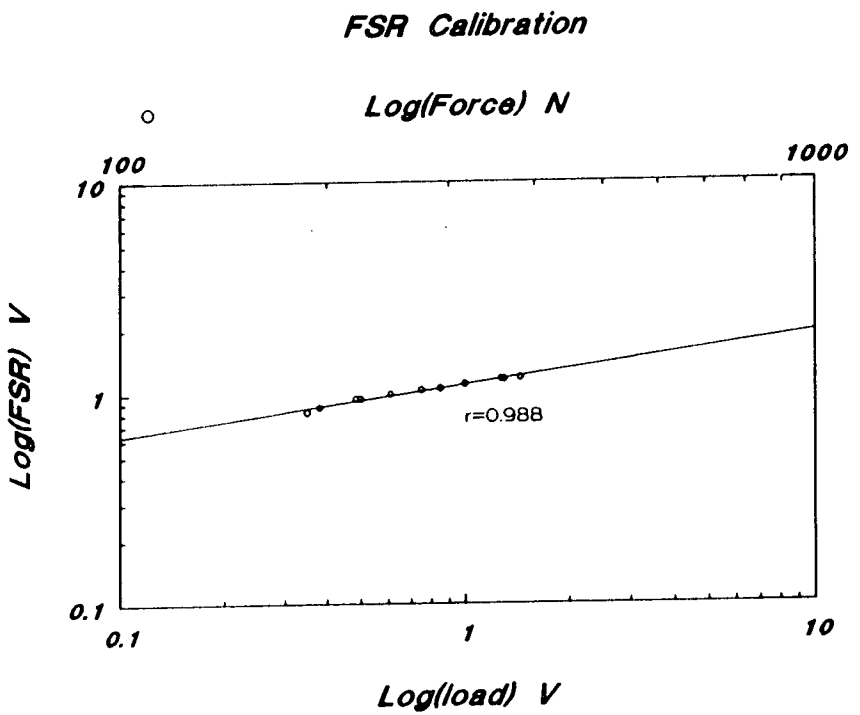
FSR Calibration
Log(Force) N
100
1000
10
1
0.1
r=0.988
0.1
1
10
Log(FSR) V
Log(load) V

Figure 3.5 Peak bite force record (N) for one subject acquired at 20sec intervals for 256sec before and after the MR exercise period. The output signal of the FSR™ is in Volts.

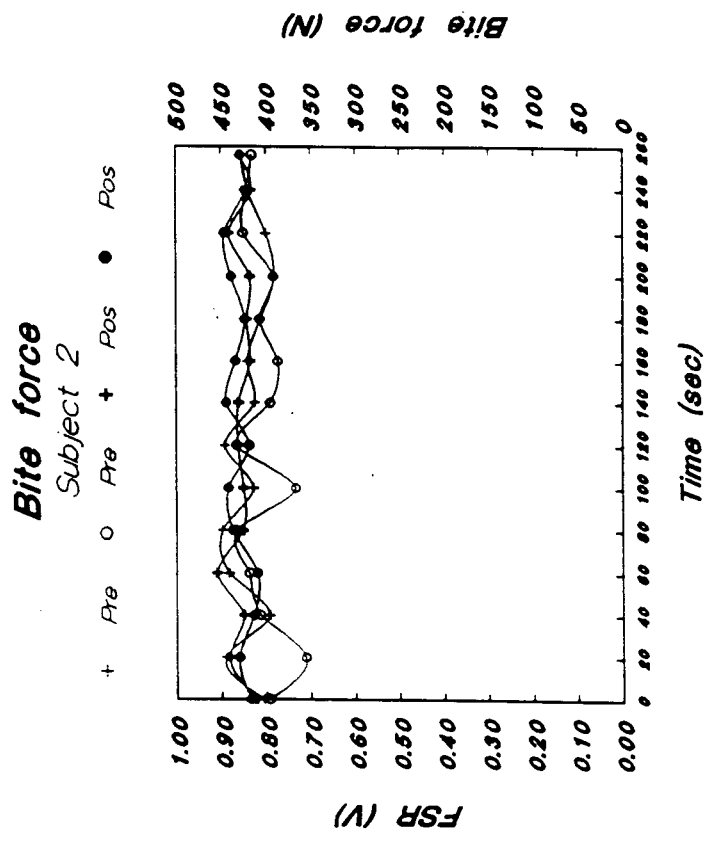
Bite force
Subject 2
+ Pre ○ Pre + Pos ● Pos
Bite force (N)
500
450
400
350
300
250
200
150
100
50
0
FSR (V)
1.00
0.90
0.80
0.70
0.60
0.50
0.40
0.30
0.20
0.10
0.00
0 20 40 60 80 100 120 140 160 180 200 220 240 260
Time (sec)

3.3.4 Magnetic Resonance Spectroscopy of Subjects

^{31}P MR spectroscopy was performed using a Philips Gyroscan S15/High Performance 1.5T superconducting system (Philips Medical Systems, Shelton CT.) operating at approximately 63MHz for ^{1}H and 25MHz for ^{31}P. Spectra were acquired from three sites in the right masseter muscle at rest, during left, and then right intermittent clenching (1sec clench, 1sec rest). A 90° excitatory RF pulse was generated for 27μsec from a custom-designed 2cm by 3cm ovoid, single turn surface coil, centred over each of the three regions. The surface coil was sensitive to a depth of approximately 1.25cm. In order to achieve an acceptable signal-to-noise ratio in the MR spectra, careful positioning of the surface coil was necessary over the region-of-interest. Unpublished observations from dissections performed in our laboratory on human cadaver material demonstrated that the muscle is separable posteriorly into three distinct layers, and inseparable anteriorly. The most superficial of these layers extends through the anterior half of the muscle only, while the next compartment, the intermediate layer, extends more posteriorly, toward the posterior border of the mandible. The deepest layer, closest to the bone, fans out from the mandible superiorly, but is exposed only anterior to the articular condyle. Site 1 was located along the anterior border of the muscle, midway between its zygomatic origin and mandibular insertion. Site 2 was located at the posterior border of the muscle, midway between the articular condyle and the gonial angle, and site 3 was located one finger's breadth anterior to the articular condyle. At each site, magnetic field homogeneity was optimized using the ^{1}H signals from water and fat by modifying current flow through the surface coil. 256 signal FIDs were accumulated at rest at each of the three positions and 128 signal FIDs were acquired during exercise at these same sites, during left, and then right, intermittent, maximal clenching. During exercise, the clenching rhythm was set by an external electronic signal which was audible to the subjects inside the MR unit. A 5min rest period was utilized between each exercise which permitted the metabolites to recover to their resting levels (Taylor et al, 1983; Jenesson et al, 1989). Measurement time utilizing a 1sec repetition time amounted to approximately 8.5mins at rest and 4.3mins during each exercise regimen.

3.3.5 Determination of Peak Saturation Factors

Saturation factors were determined for three subjects by comparing the signal areas of the P_i and PCr peaks utilizing 1sec and 10sec repetition times. If the nuclei are not allowed to return to their fully relaxed equilibrium state (approximately 4.017sec and 5.517sec for T_1 relaxation for P_i and PCr, respectively (Thomsen, Jenesen and Henriksen, 1989)), before the application of another excitatory RF pulse, then the MR signal will be decreased in amplitude (Axel, 1984). For the pulse widths and powers used, the saturation factors for the P_i and PCr peaks were 1.11±0.17 and 1.40±0.20, respectively (i.e. the P_i and PCr signals were reduced by 11% and 40%, respectively). The data presented have been corrected for the effects of saturation.

3.3.6 Quantification of ^{31}P Magnetic Resonance Spectra

Following acquisition, the spectra were transferred to a VAX 11/750 computer (Digital Equipment Corp., Maynard, MASS.) and displayed on a Ramteck RM9645 graphics display system (Ramteck Corporation, Sunnyvale, CA.). These spectra were transformed using Fourier techniques and phase- and baseline corrected using custom-designed software. A Gaussian function was then fitted to each spectral peak and from this, peak areas and positions (in ppm) were calculated. Absolute metabolite concentrations cannot be obtained directly without knowing the volume of muscle within the range of the surface coil (Taylor et al, 1983). Therefore the concentration of inorganic phosphate (P_i) is given in normalized units: $P_i/(PCr+P_i)$, (Taylor et al, 1983). The PCr concentration is equal to $PCr/(PCr+P_i)$, in normalized units. The relative metabolic activity in the muscle is given by the ratio, P_i/PCr (McCully et al, 1988) and pH is calculated from a calibration curve which is expressed as

$$pH = 6.75 + \log_{10}[(\sigma-3.27)/(5.69-\sigma)]$$

where σ is the chemical shift between the P_i and PCr peaks in ppm (Taylor et al, 1983). While peak position may be measurable to an accuracy of 0.02ppm, an error as great as 0.1 pH units may occur during these calculations (Gadian et al, 1979; Chance et al, 1986).

3.3.7 Statistical Techniques

Statistical analyses were performed using single factor ANOVA and Tukey HSD tests. The null hypothesis was rejected at the 0.05 level of significance.

CHAPTER 4

Results

4.1 Three-Dimensional Computer Reconstruction of Tendon Planes in Human Masseter Muscle

Sagittal cryosectioning of the cadaver masseter muscle revealed a total of five major tendon or connective tissue inscriptions in the muscle. The first of these was seen in the first millimetre cryosection bordering the zygomatic arch superior to the deep masseter muscle. This inscription extended as far medially as slice 11. A second inscription appeared in the third millimetre cryosection and bordered the inferior border of the deep part of the deep masseter until the tenth millimetre. In the eleventh millimetre, this inscription became discontinuous near its midpoint. However, in the seventeenth millimetre, the two parts became continuous again. Between the eighteenth and twenty-eighth millimetre cryosections, the inscription was reduced to a small band of tissue near the posterior border of the muscle only and disappeared from view soon thereafter.

A third small inscription was seen in the fourth millimetre cryosection, along the posterior border of the muscle nearer the gonial angle of the mandible. Initially, the inscription was directed inferiorly until the fifteenth millimetre cryosection. Deeper, this inscription coursed superiorly into the muscle between two inscriptions which had bony attachments on the zygomatic process of the maxilla. Another small inscription was observed near the inferior border of the muscle at slice fifteen. The two appeared to become continuous in slice twenty-eight, but the smaller one disappeared from view after slice thirty-five.

A heavy inscription was seen on the anterior border of the cadaver masseter muscle, attached to the zygomatic process of the maxilla. Nearer the maxillary attachment, the inscription appeared thick and heavy, thinning into the muscle mass. In slice two it

extended two-thirds of the way down the anterior border of the muscle adjacent to glandular tissue, which might possibly be the accessory parotid gland. In slice ten, it extended the entire distance of the anterior border of the muscle. The length of this inscription varied throughout the remainder of the muscle slices, shortening and then lengthening again, but was visible as far medially as the forty-fifth slice, although it was much reduced in size.

Another inscription, with an area of attachment slightly superior to the previous one on the zygomatic process of the maxilla extended inferiorly into the muscle, and appeared to divide the superficial muscle into two near-equal halves, superio-inferiorly. This inscription, was also thick near its bony attachment and thinned inferiorly as it tracked into the muscle mass. It was not seen after slice twenty-eight.

Five tendinous or connective tissue inscriptions were also apparent from coronal cryosections obtained approximately half-way through the cadaver masseter muscle. The most medial of these appeared anchored to the coronoid process of the mandible defining the most medial border of the deep masseter muscle. An inscription dividing the deep part of the muscle from the superficial part was also seen. In the superficial part of the muscle, a thick inscription was observed extending approximately half-way down the lateral border of the muscle adjacent to glandular tissue. Another inscription, running parallel to this one, also anchored to the zygomatic processes of the maxilla, was seen extending inferiorly into the muscle. A small triangular shape inscription, the most inferior of the three was seen anchored to the mandibular corpus, extending superiorly.

Three-dimensional computer reconstruction of the cadaver masseter muscle revealed a series of five interdigitating tendon sheets. It is apparent from the reconstruction that sehnenspiegel 1, the most superficial of the five, covers the anterior, lateral, and a portion of the medial surface of the muscle. Sehnenspiegel 2, which has a ramal attachment, is directed superiorly, and then medially to sehnenspiegel 1. Sehnenspiegel 3

has a zygomatic attachment near sehnenspiegel 1. This tendinous inscription courses inferiorly, and then medially to sehnenspiegel 2. Sehnenspiegel 4 come has a mandibular attachment, midway along the posterior border of the mandibular ramus, and is directed more anteriorly. Sehnenspiegel 5, the most medial and superior of the five is the medial-most border between the deep part of the muscle and temporalis. Figure 4.1 represents true lateral views of the muscle tendons (gold) without, and with the muscle outline (red), while Figure 4.2 represents the medial view of the same muscle.

A software-aided cut section of the computer-reconstructed masseter muscle was generated in the coronal plane near the posterior border of the muscle. At this level of section, four tendon planes are visible on the cut computer-generated muscle. Sehnenspiegel 1 is seen as a small inscription near the lateral border of the muscle. Sehnenspiegel 2 is a thicker inscription seen near the inferior border. Sehnenspiegel 4 and 5 are visible extending near the top of the muscle (Figure 4.3, left). On the corresponding MR image, sehnenspiegel 2, 4 and 5 are visible as low-signal intensity regions, however, the latter two are adjacent to high-signal intensity regions. Sehnenspiegel 1 is not visible as a low-intensity signal band (Figure 4.3, right).

Figure 4.1 Lateral view of a three-dimensional computer reconstruction of the cadaver masseter muscle with condylar head. The condylar head is depicted in ivory with masseter muscle tendon sheets in gold without (top) and with (bottom) the muscle outline. In both cases, the scale bar represents 1cm.

Figure 4.2 Medial view of a three-dimensional computer reconstruction of the cadaver masseter muscle with condylar head. The condylar head is depicted in ivory with masseter muscle tendon sheets in gold without (top) and with (bottom) the muscle outline. In both cases, the scale bar represents 1cm.

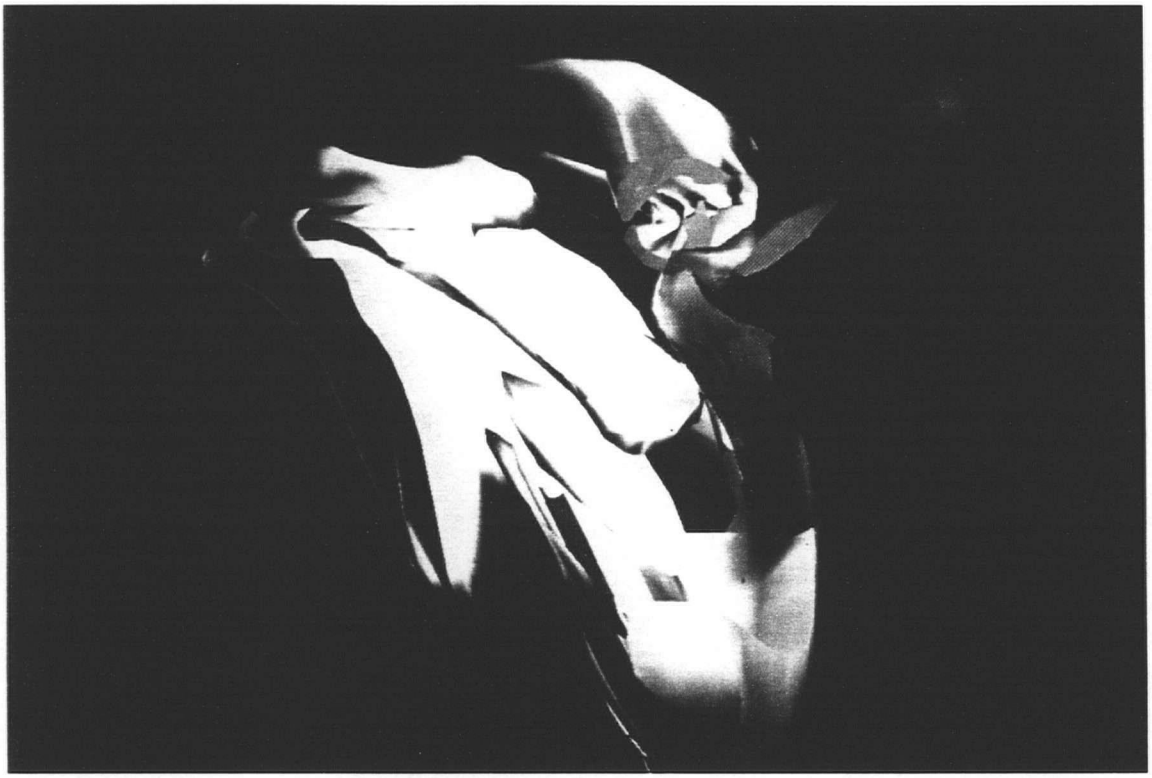

Figure 4.3 Computer-generated, software cut section through the posterior portion of the cadaver masseter muscle (left) and the corresponding MR section (right). The scale bar represents 1cm.

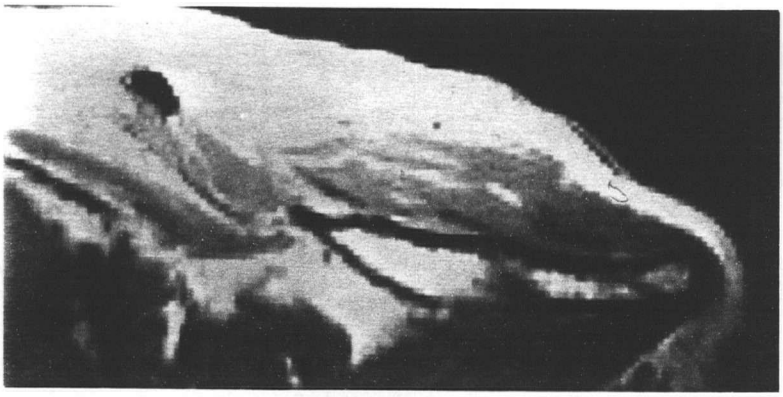

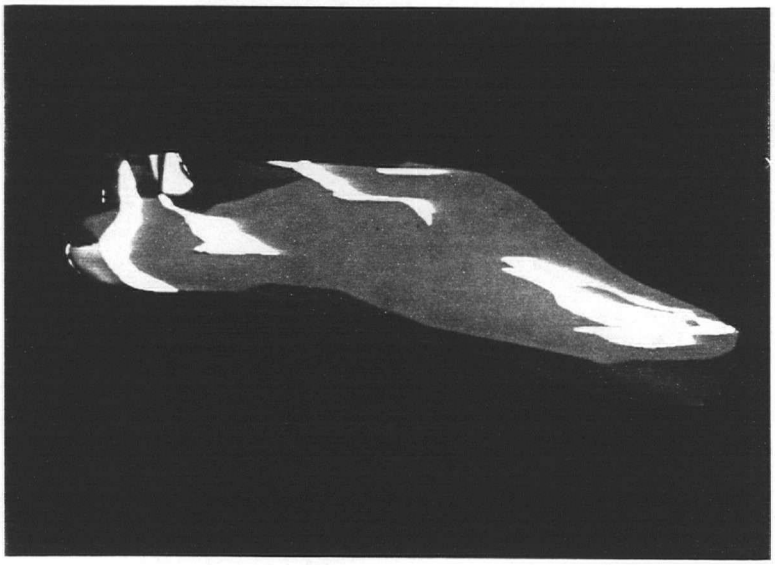

4.2 Estimation of Tendon Plane Orientation within Human Masseter Muscle from Reconstructed Magnetic Resonance Images

4.2.1 Cephalometry

Data derived from cephalometric radiography, as well as bizygomatic and bigonial measurements are shown in Table 4.1. These data are typical of a modern, randomly selected adult population. Some particularly large variations in a craniofacial form were found. Subject 2, for example, had a relatively large ANB angle of 8.5°. Subject 5 had a comparatively long mandible and maxilla, high lower face and flat mandibular plane angle. As bizygomatic and bigonial measurements were equally large, this subject possessed a relatively narrow masseteric "muscle width". In contrast, subject 4, who had the shortest ramus and lower face height had a similar "masseteric width" due to near equal bizygomatic and bigonial widths. Subject 1, whose craniometric measurements were generally intermediate between those of subjects 4 and 5, had the largest bizygomatic width, and hence the largest "masseteric width" (Brown, 1973).

4.2.2 Magnetic Resonance Imaging of Subjects

Adipose tissue produces the highest intensity signal on spin-echo MR images, given its proton density, and T_1 and T_2 relaxation times. In contrast, tendon is a weak-signal-producing tissue and appears black. Muscle tissue is intermediate in intensity (Pavlicek et al, 1984) (Figure 4.4B). The relative intensities of the tissues appeared to be unaffected by magnetic field strength, or image display parameters. Muscle and tendon outlines were identified on each MR image, but only muscle outlines were traced from these sections onto acetate overlays leaving voids in areas identified as tendon. This was easy to accomplish due to the different signal characteristics of the two tissues.

In accordance with the descriptions of Ebert (1939) and Schumacher (1961), muscle compartments appeared to be layered medio-laterally. In the superior-inferior dimension, the superficial layer inserted near the inferior border of the mandible and the deepest layer

inserted nearer the coronoid notch. This arrangement was also noted by Schumacher (1961). While the superficial and intermediate muscle compartments were evident in the most posterior MR slices, the deepest muscle layer was not seen until the third or fourth slice from the rear. The intermediate compartment spanned the posterior five or six coronal slices, while the deep layer spanned only three in the middle of the muscle. Toward the anterior of the muscle, its division by tendon was unresolvable, giving the impression that the muscle layers were either fused (as suggested by DuBrul, 1980; McMinn et al, 1981), or that the tendon planes became oriented paracoronally, as is the case in the pig (Herring and Scapino, 1973).

4.2.3 Muscle Breadth Measurements

The breadth of the superficial, intermediate and deep muscle compartments is tabulated in Table 4.2. It is apparent that the widths of the intermediate and deep parts were relatively constant for all subjects, except for subject 3, whose deep compartment was particularly wide (9.1mm). Subject 5 displayed the largest superficial masseter (10.8mm) while subject 4 possessed the smallest.

Table 4.1

Skeletal Parameters by Subject

Values include individual measurements, group means, Standard Deviations and Coefficients of Variation.

Subject	1	2	3	4	5	Mean	SD	CV
Variable								
Ant. pos. of maxilla	81.0°	78.3°	91.0°	78.5°	88.0°	83.4°	5.8°	-
Ant. pos. of mandible	79.8°	74.5°	82.5°	74.3°	85.0°	79.3°	4.8°	-
Cranial base angle	135.5°	141.7°	127.5°	131.0°	129.0°	132.9°	5.8°	-
Gonial angle	127.3°	130.8°	126.5°	127.5°	122.0°	126.8°	3.0°	-
Palatal angle	11.0°	14.0°	8.0°	9.0°	3.0°	9.0°	4.1°	-
Mandibular plane angle	26.0°	25.0°	23.3°	27.3°	18.3°	24.0°	3.5°	-
Ramal length (cm)	6.0	5.2	5.0	4.3	5.6	5.2	0.6	11.5%
Mandibular length (cm)	7.5	8.5	7.2	7.2	9.2	7.9	0.9	11.4%
Maxillary length (cm)	5.6	6.1	6.7	6.2	7.3	6.2	0.7	10.6%
Upper facial ht. (cm)	5.9	6.3	5.4	5.6	5.6	5.8	0.4	6.9%
Lower facial ht. (cm)	7.0	7.4	6.6	5.4	8.1	6.9	1.0	14.5%
Cranial base len. (cm)	10.7	12.1	10.1	10.1	12.1	11.0	1.0	9.1%
Ant. cran. base len.	6.3	8.3	7.0	7.2	8.1	7.4	0.8	10.8%
Bizygomatic width (cm)	13.8	12.9	12.6	11.0	13.0	12.7	1.0	7.9%
Bigonial width (cm)	10.8	10.9	10.8	9.2	11.2	10.6	0.8	7.4%
Masseteric width (cm)	1.5	1.0	0.9	0.9	0.9	1.0	0.3	25.1%

Table 4.2

Mean Compartment Breadths by Subject

Subject	Superficial Compartment (mm)	Intermediate Compartment (mm)	Deep Compartment (mm)
1	6.6±2.1	5.4±2.0	7.0±0.5
2	7.5±2.8	6.7±1.9	6.2±2.1
3	9.6±3.5	6.2±3.9	9.1±2.1
4	7.2±2.9	7.4±1.7	6.1±2.5
5	10.8±3.5	7.4±3.0	6.2±1.6

Figure 4.4 Coronal cryosection, magnetic resonance image and line tracing of a section through a left human masseter muscle.
A) Coronal cryosection of a left masseter muscle (M), tendon (small arrows) and mandibular ramus (R) from a human cadaver head. The scale bar represents 1cm.
B) Coronal 5mm magnetic resonance image of a left masseter muscle near the same anatomic level of sectioning as (A). The image was obtained at 1.0T using a head coil and spin-echo (SE500/17). The scale bar represents 1cm.
C) Line tracing of the magnetic resonance image depicted in (B). The scale bar represents 1cm.

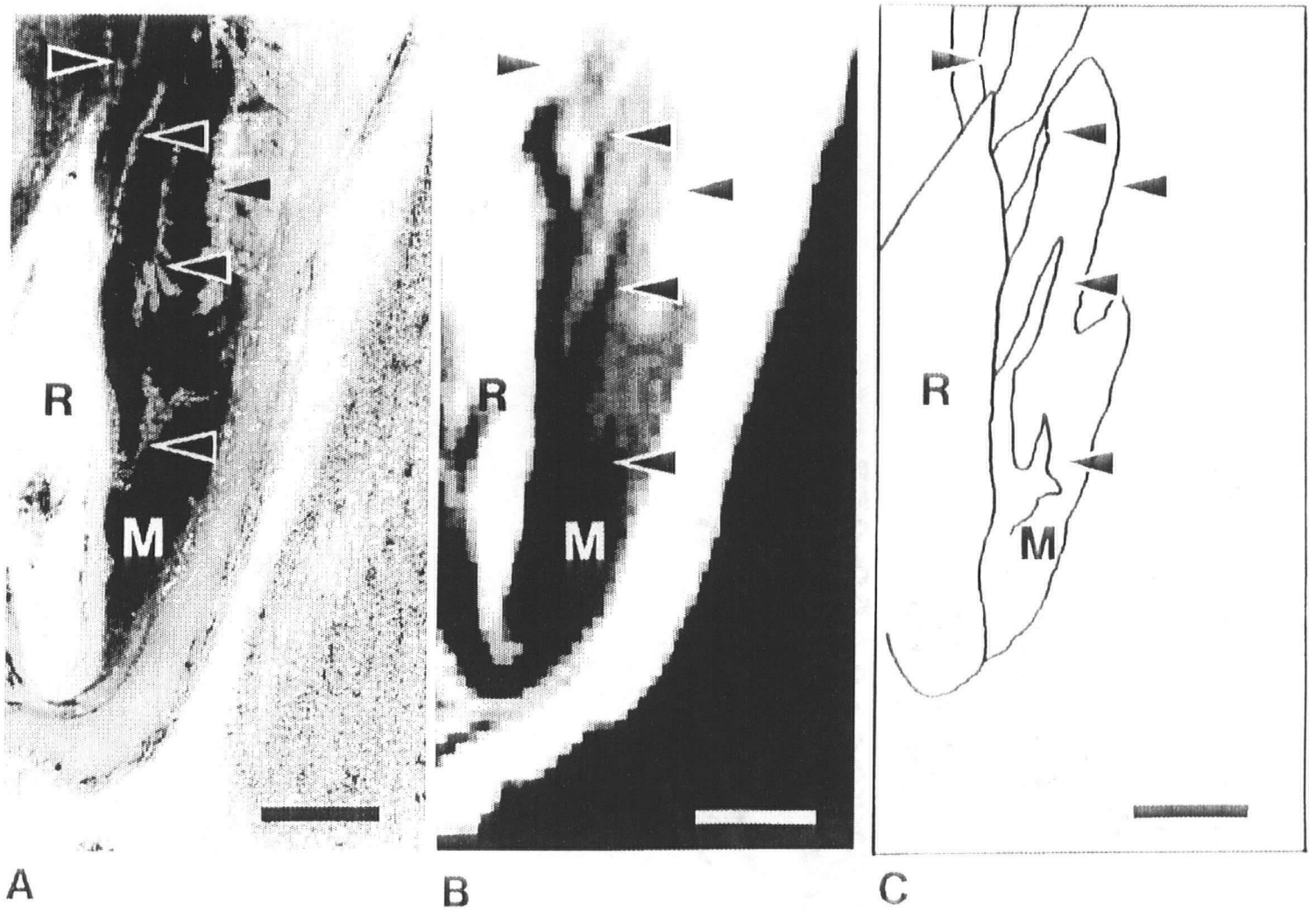
R
M
A
R
M
B
R
M
C

4.2.4 Three-dimensional Computer Reconstructions

Four tendon planes were identified for each masseter muscle. Plane (I), the most lateral, was anchored to the zygomatic arch and extended inferiorly onto the lateral surface of the muscle. Plane (II) was attached to the mandibular ramus and extended superiorly into the muscle. Plane (III) was attached to the zygomatic arch, more medial than plane (I), and extended inferiorly into the muscle. Plane (IV), the most medial of the tendon planes, was located on the inner, or deep surface of the muscle (Figure 4.5).

4.2.5 Tendon Plane Angle Estimation

Table 4.3 shows the mean three-dimensional angulations of the tendon planes and their standard deviations, measured relative to the mid-sagittal plane, both coronally and axially. In the coronal view, our convention was such that a positive angle was one which was measured clockwise relative to the mid-sagittal plane. In the coronal view, planes I and IV demonstrated the greatest mean angulation (-9.7°±4.3° and -23.9°±5.6°, respectively). The two intramuscular planes, II and III, were nearly vertically oriented (3.0°±4.4° and -1.0°±8.3°, respectively). In the axial view, the mean angulation of plane IV was the greatest (15.3°±8.1°) compared to the other planes. Collectively, our data demonstrated that the attachment sites of the muscle fibres on the tendon faces orientation differs from one muscle compartment to the next when viewed in three-dimensional space.

To assess the overall error of the tendon plane angle estimation process, one subject was imaged on two separate occasions by MRI using the protocol outlined earlier. The tendon plane angulation data derived for this subject following the second determination are shown enclosed in brackets in Table 4.3. The individual differences between subsequent tendon plane angle estimations varied between 0.5° and 9.1° (mean 5.5°).

Figure 4.5 Three-dimensional computer reconstruction of a right human masseter muscle from magnetic resonance images viewed coronally from the rear of the muscle. Three muscle compartments and three fitted tendon planes are shown. The scale bar represents 1cm.

Table 4.3

Mean Angulations of Tendon Planes Relative to the Mid-Sagittal Plane by Subject

Individual measurements, group means and Standard Deviations are shown for both coronal and axial views.

Plane	Subject	Coronal View Angulation	Axial View Angulation
I	1	- 6.5° (- 10.9°[1])	- 17.3° (- 15.5°)
	2	- 15.7°	- 12.1°
	3	- 6.0°	1.5°
	4	- 12.8°	- 18.2°
	5	- 7.8°	3.4°
II	1	2.3° (- 6.7°)	4.8° (- 0.8°)
	2	3.7°	- 1.3°
	3	0.1°	16.4°
	4	- 1.1°	16.0°
	5	10.1°	9.9°
III	1	- 11.8° (12.3°)	- 4.3° (4.8°)
	2	8.1°	7.7°
	3	0.2°	- 17.5°
	4	- 7.0°	- 6.6°
	5	5.1°	- 11.9°
IV	1	- 29.6° (- 34.4°)	7.7° (- 0.8°)
	2	- 26.3°	12.0°
	3	- 19.5°	26.8°
	4	- 16.5°	20.4°
	5	- 27.6°	9.5°

Group means (n=5)	X	SD	X	SD
I	- 9.7°	4.3°	- 9.9°	8.7°
II	3.0°	4.4°	9.2°	7.5°
III	- 1.0°	8.3°	- 6.5°	9.4°
IV	- 23.9°	5.6°	15.3°	8.1°

[1]Measurements enclosed in brackets represent tendon plane angle determinations of subject 1 using MRI data acquired following a second imaging session.

4.3 Regional ^{31}P Magnetic Resonance Spectroscopy of Exercising Human Masseter Muscle

4.3.1 Quantification of ^{31}P Magnetic Resonance Spectra

Figures 4.6a, b and c show typical resting ^{31}P MR spectra acquired from the anterior superficial, posterior intermediate and deep parts of the right masseter muscle, obtained from 256 signal acquisitions over an 8.5min time period. The resonance peaks observed from left to right are: the 0.1mM methylenediphosphonic acid standard (Aldrich Chemical Co., Milwaukee, WI.), phosphomonoester (PME), inorganic phosphate (P_i), phosphodiester (PDE), creatine phosphate (PCr) and the γ-, α- and β- phosphorous nuclei of ATP. The phosphomono- and diesters are particularly prominent signals in the head and neck region (Vogl et al, 1989) and are not readily observed in the limbs (e.g. McCully et al, 1988). These constituents represent the precursors of membrane biosynthesis, in particular, phosphorylcholine, phosphorylethanolamine and sugar phosphates, and hexose phosphate, respectively (Taylor et al, 1983; Meyer et al, 1985). For these spectra, the P_i/PCr ratios in the three sites were 0.27, 0.30 and 0.51, respectively, and the pH values are 7.17, 7.22 and 7.17, respectively.

During exercise, there is an increase in the P_i peak area due to a net breakdown of PCr. As well, there is a decline in pH, presumably due to the accumulation of lactic acid. This type of change has been reported in the limb muscles, and quantitatively, while large variations in PCr breakdown have been observed, the relationship between pH and the decrease in PCr concentration is highly reproducible (Taylor et al, 1983). The spectra shown in Figures 4.7a, b and c were obtained from the same subject and at the same sites as that of Figure 4.6, but during intermittent left molar clenching. The P_i/PCr ratios for these spectra were 1.16, 1.68 and 3.38, respectively, for the three sites. The corresponding pH values were 7.01, 6.88 and 6.97. During intermittent right sided molar clenching, the P_i/PCr ratios were 1.91, 1.71 and 2.32 for the three sites respectively, while the pH values were 6.86, 6.82 and 6.97, respectively. For these spectra, see Figure 4.8a,b and c.

In the anterior superficial part of the muscle, the mean P_i/PCr ratio increased from 0.40±0.13 at rest to 1.09±0.47 to 1.23±0.77 for left and right molar clenching, respectively. These differences were significant to $p<0.05$. This corresponded to an increase in mean free [P_i] from 0.29±0.06 to 0.50±0.13 and to 0.50±0.20 for left and right molar clenching, respectively. These differences were also significant to $p<0.05$. Mean pH decreased from 7.14±0.08 to 7.01±0.11 and to 6.99±0.08, respectively.

In the posterior intermediate part of the muscle, the mean P_i/PCr ratio increased from a resting level of 0.42±0.11 to 1.23±0.67 and to 1.30±0.54 for left and right molar clenching, respectively. These differences were significant to $p<0.05$. Mean free [P_i] increased from 0.29±0.05 to 0.54±0.10 and to 0.49±0.16 for these same clenching tasks, respectively. These differences were significant to $p<0.01$. Mean pH also decreased with exercise from 7.11±0.06 to 7.00±0.09 and to 7.01±0.10, respectively.

The deep part of the muscle displayed both a higher mean resting P_i/PCr ratio of 0.70±0.17 and mean [P_i] of 0.41±0.06 than the other two sites. Both differences were significant to $p<0.01$. The mean P_i/PCr ratio increased to 1.70±0.89 and to 1.54±0.60 for left and right molar clenching, respectively. Mean [P_i] increased to 0.58±0.11 and to 0.59±0.10. This difference was significant to $p<0.01$. Mean pH decreased from 7.17±0.03 at rest to 7.03±0.06 and to 7.03±0.05. These differences were significant to $p<0.001$. The results are summarized in Table 4.4.

Table 4.4

Relative concentrations of metabolites and pH (means±SD)
from three sites in the right human masseter muscle
at rest and during left and right molar clenching

Individual values were corrected for saturation effects before averaging

Site	Rest			Left molar clench			Right molar clench		
	P_i/PCr	P_i/P_{tot}	pH	P_i/PCr	P_i/P_{tot}	pH	P_i/PCr	P_i/P_{tot}	pH
1	0.40±0.13	0.29±0.06	7.14±0.08	1.09±0.47	0.50±0.13	7.01±0.11	1.23±0.77	0.50±0.20	6.99±0.08
2	0.42±0.11	0.29±0.05	7.11±0.06	1.23±0.67	0.54±0.10	7.00±0.09	1.30±0.54	0.49±0.16	7.01±0.10
3	0.70±0.17	0.41±0.06	7.17±0.03	1.70±0.89	0.58±0.11	7.03±0.06	1.54±0.60	0.59±0.10	7.03±0.05

Organic phosphate (P_i), creatine phosphate (PCr), total phosphate ($P_{tot}=P_i+PCr$)

Figure 4.6 ^{31}P Magnetic resonance spectra of human masseter muscle at rest corresponding to the anterior superficial (a), posterior intermediate (b), and deep (c) parts of the muscle. The positions of the MDA (1), phosphomonoester (PME) (2), inorganic phosphate (P_i) (3), phosphodiester (PDE) (4), creatine phosphate (PCr) (5) and the γ - (6), α- (7) and β-(8) phosphorous nuclei of ATP resonance peaks are shown for spectrum (a) only. For spectrum (a), the P_i/PCr ratio is 0.27, the [P_i] is 0.21 and the pH is 7.17. For spectrum (b), the P_i/PCr ratio is 0.30, the [P_i] is 0.23 and the pH is 7.22. For spectrum (c), the P_i/PCr ratio is 0.51 the [P_i] is 0.34 and the pH is 7.17.

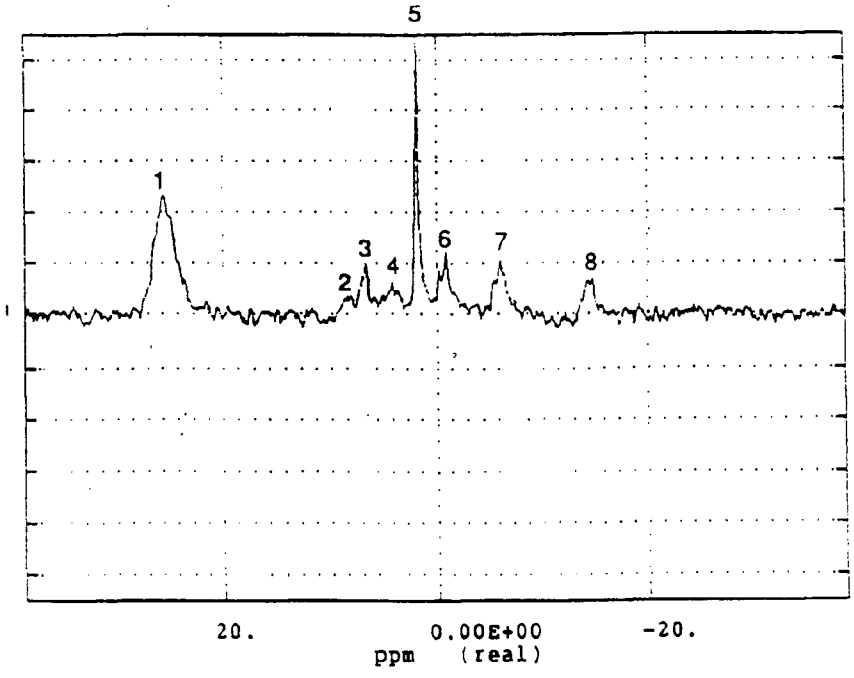

a

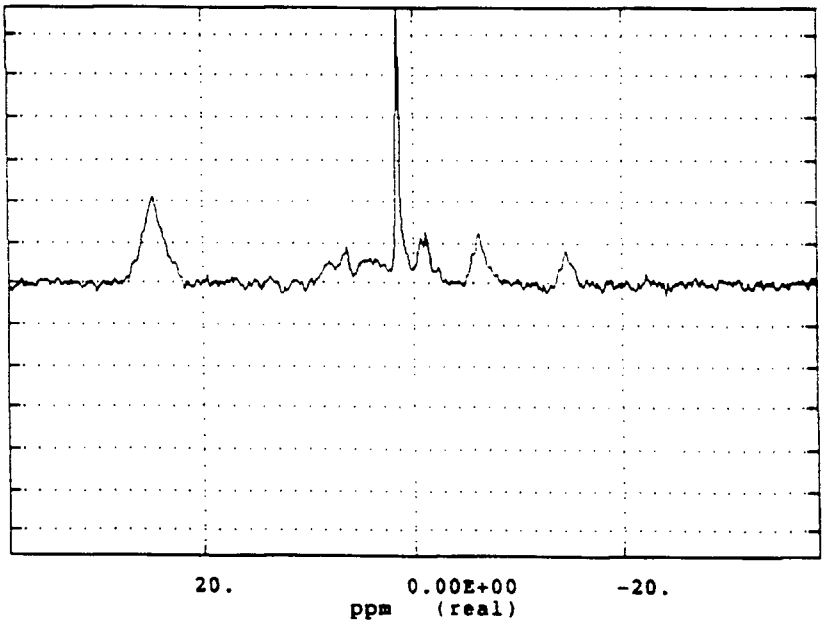

b

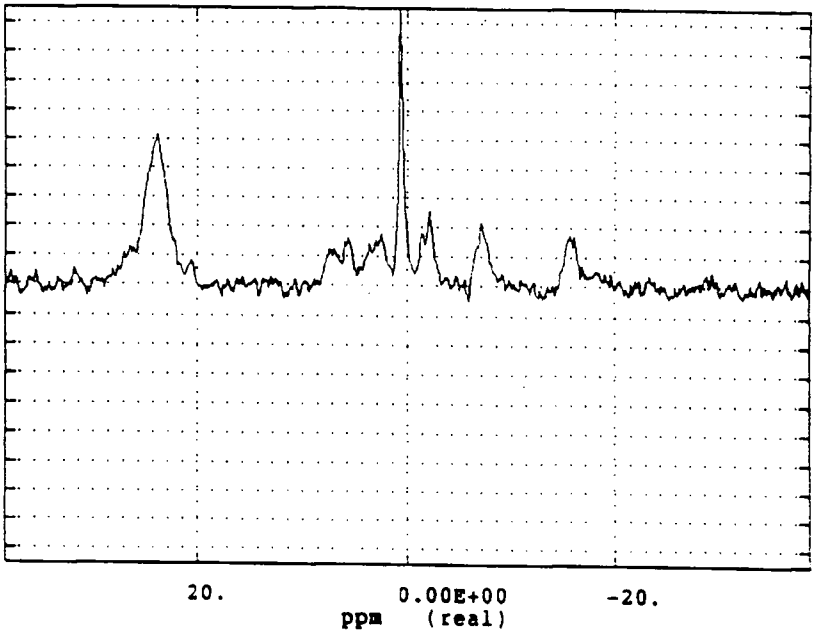

C

Figure 4.7 ^{31}P Magnetic resonance spectra of human masseter muscle during intermittent, left molar clenching corresponding to the anterior superficial (a), posterior intermediate (b), and deep (c) parts of the muscle. For spectrum (a), the P_i/PCr ratio is 1.16, the $[P_i]$ is 0.54 and the pH is 7.01. For spectrum (b), the P_i/PCr ratio is 1.68, the $[P_i]$ is 0.63 and the pH is 6.88. For spectrum (c), the P_i/PCr ratio is 1.90, the $[P_i]$ is 0.52 and the pH is 6.97.

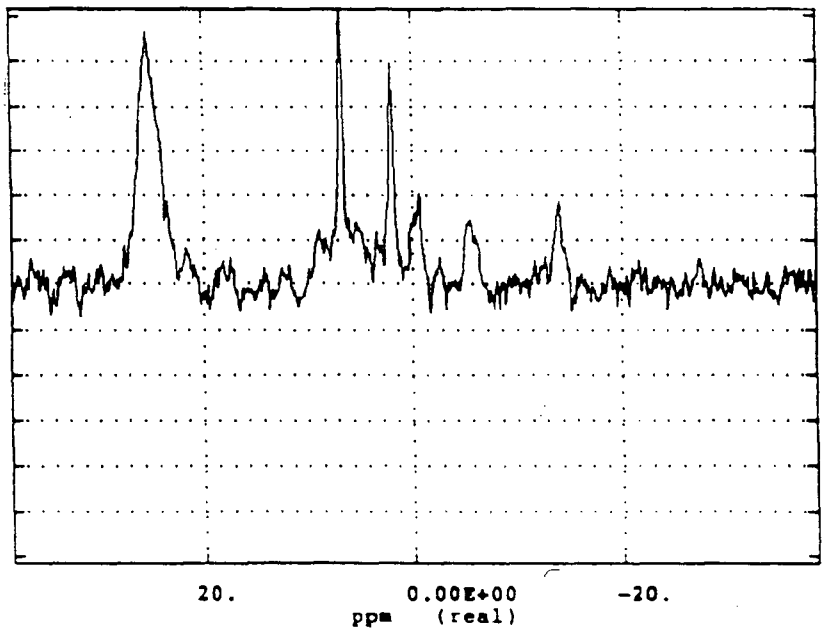

a

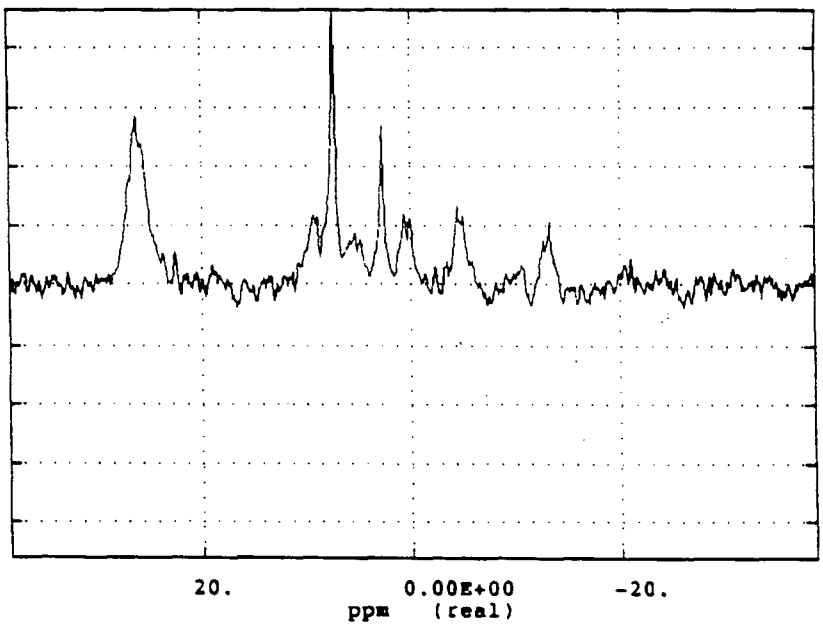

b

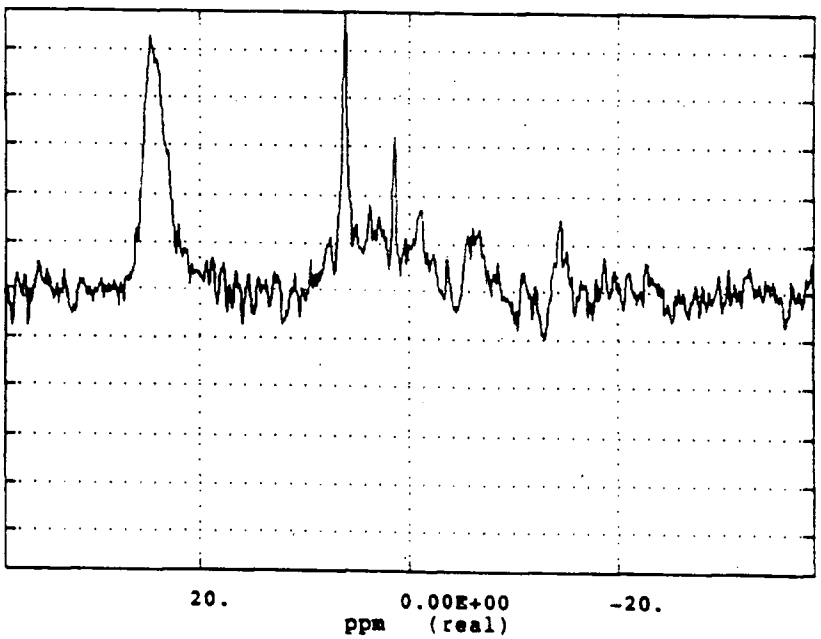

C

Figure 4.8 ^{31}P Magnetic resonance spectra of human masseter muscle during intermittent, right molar clenching corresponding to the anterior superficial (a), posterior intermediate (b) and deep (c) parts of the muscle. For spectrum (a), the P_i/PCr ratio is 1.91, the [P_i] is 0.66 and the pH is 6.86. For spectrum (b), the P_i/PCr ratio is 1.71, the [P_i] is 0.63 and the pH is 6.82. For spectrum (c), the P_i/PCr ratio is 2.32, the [P_i] is 0.70 and the pH is 6.97.

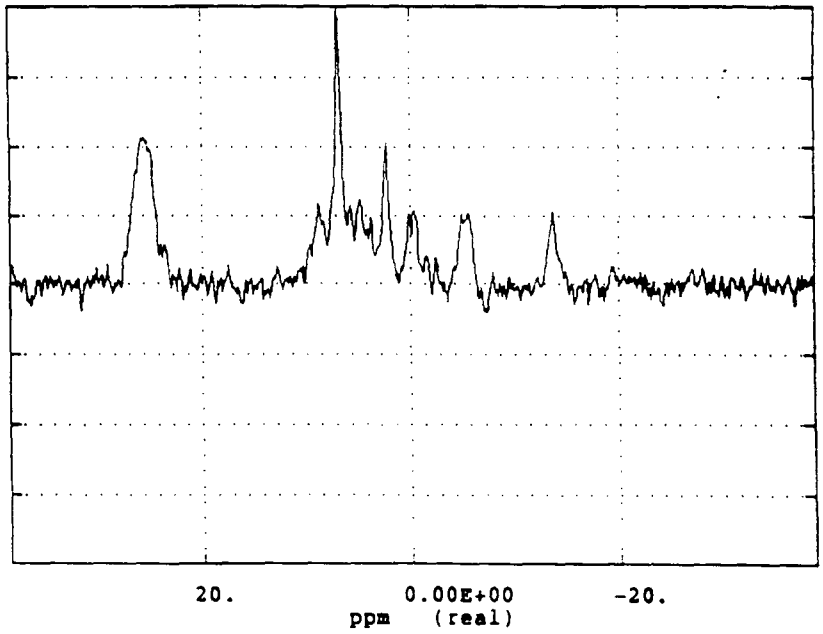

a

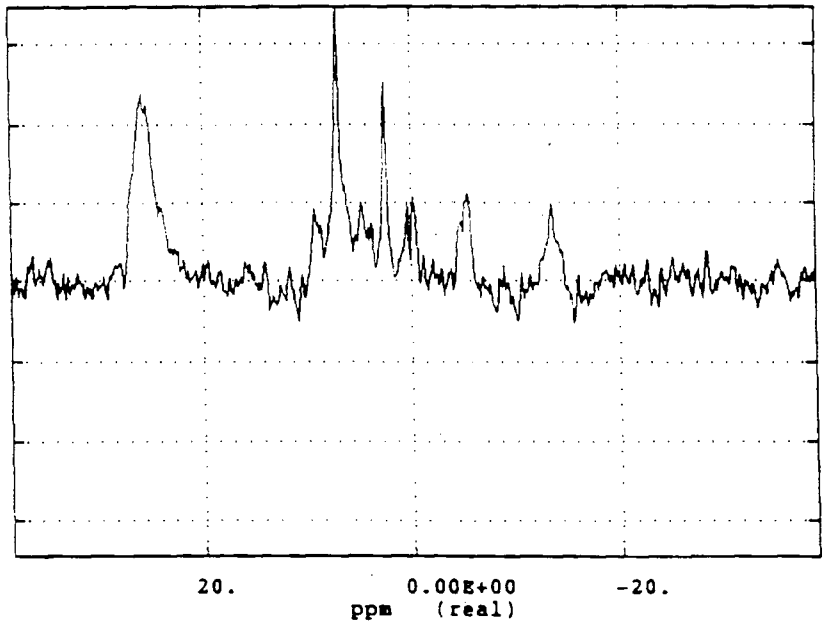

b

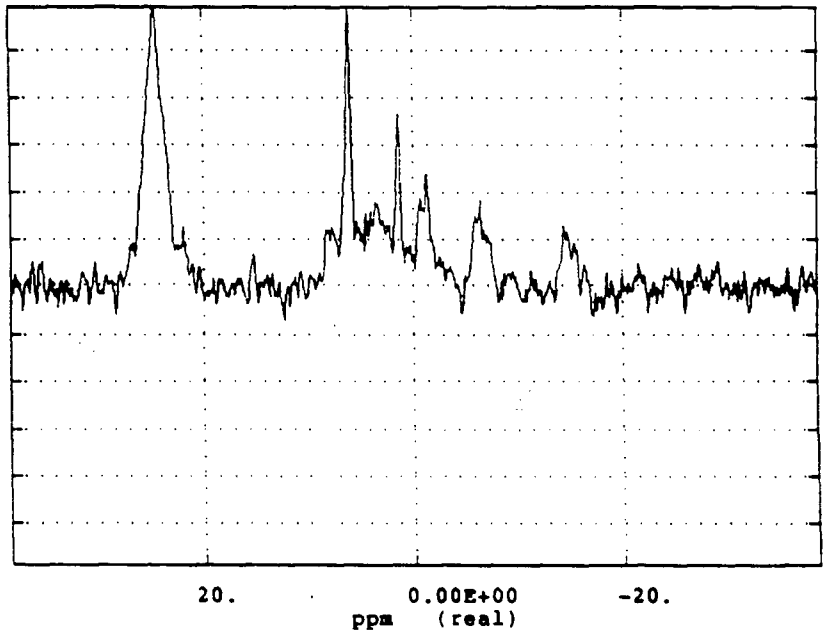

C

CHAPTER 5

Discussion

5.1 Discussion of the Methods

5.1.1 Cryosectioning and Computer Reconstruction of the Cadaver Masseter Muscle

Sagittal cryosectioning of the cadaver masseter muscle generated forty-five 1mm sections through the muscle. Like Schumacher (1961a) five sehnenspiegel, or tendon planes, were identified in the muscle. Of the five, the most lateral inscription was the thickest, covering greater than half the muscle body laterally, medially, as well as anteriorly. Sehnenspiegel 3, having an attachment near sehnenspiegel 1 on the zygomatic process of the maxilla, was equally thick and heavy but coursed directly into the muscle body. Sehnenspiegel 2 and 4 had ramal attachments and were, in general, finer inscriptions directed into the muscle body between sehnenspiegel 1 and 3, and 3 and 5, respectively. Sehnenspiegel 4 also appeared to delineate the deep masseter from the other surrounding structures. These observations were also corroborated in the limited number of coronal cryosections which were obtained near the antero-posterior midpoint of the muscle.

5.1.2 Magnetic Resonance Imaging

To date, the use of magnetic resonance imaging (MRI) as a tool for investigating the craniomandibular tissues has been limited (Unger, 1985; Seltzer and Wang, 1987; van Spronsen et al, 1987; Hannam and Wood, 1989; Koolstra et al, 1990; Schellhas, 1990), although there have been numerous MRI investigations of the temporomandibular articulation (Harms et al, 1985; Roberts et al, 1985; Helms et al, 1986; Katzberg et al, 1986; Westesson et al, 1987). While x-ray computed tomography has proved a satisfactory method for tissue imaging by multiple slices in the past, its major drawback, radiation dosage has limited the number and scope of studies in the region (Weijs and Hillen, 1984; Seltzer and Wang, 1987).

A critical factor governing MR image quality is the ratio of the tissue signal to background noise. Noise is evident as diffuse areas of relative high signal intensity (white) superimposed on the image. This superimposition has the effect of blurring tissue boundaries and contours making normally homogeneous regions of tissue appear inhomogeneous. The image signal-to-noise (S/N) may be improved in three ways. The first of these is by increasing magnetic field strength. Since the total signal produced in the MR experiment is proportional to the square of the static field (Herfkens and Johnson, 1985), a finite increase in magnetic field strength will improve S/N. The generation of eddy currents in the body caused by the higher frequency RF fields needed to induce energy transitions at high magnetic field strengths have several potentially hazardous effects. These can conceivably induce local attenuations in the RF field and lead to artifacts in the MR images. The eddy currents may also pose a significant problem related to tissue heating.

The use of a fixed receiver coil, which has been demonstrated previously in the orofacial region (Unger, 1985; Seltzer and Wang, 1987; van Spronsen et al, 1987; Hannam and Wood, 1989; Koolstra et al, 1990; Schellhas, 1990) produces signals of even distribution throughout an entire slice. Image S/N may be increased when closely coupled receiver coils, or surface coils, are used in placed of the fixed units (Bydder et al, 1985). An accompanying improvement in image quality is also expected. The 10cm, dual-turn, circular surface coil which was employed provided acceptable S/N as far medially as the cranial attachment of the medial pterygoid muscle. As the imaging process is based on the repetitive acquisition of data, the third variable which can be altered to improve image S/N is number of signals acquired. This variable, as well as two additional ones determine imaging time. They are, the spatial resolution along one axis of the object, and the repetition time, T_R, described earlier. A corollary of the long imaging time is the need for the subject to remain motionless for long periods. The spatial resolution N, commonly 256, is fixed, while long T_R's contribute to excessive imaging times. Therefore, the number of signals acquired n, has the greatest impact on image S/N with improvements increasing as $\sqrt{n}$. Therefore

four signal averages were chosen throughout image acquisition.

5.1.3 Anatomical Verification of the MR Imaging Technique

As MR images represent signal averages through volumes of tissue space, a true anatomical verification of the technique is difficult unless infinitely thin MR sections are acquired. These would be impossible to obtain given the nature of acquisition process. The cadaver specimen which was imaged was milled at 1.0mm intervals so that theoretically, each 5mm MR image was acquired from the summed MR signal of five anatomical tissue sections. As photographs of the milled specimen have no extensions in depth it is conceivably difficult to compare it to an MR image which does. Therefore direct point-to-point comparisons of minor details between the photographs and the images were not always possible. In complex regions, more than one cryosection is usually necessary in order to present the morphology contained in a single MR image (Rauschning et al, 1983).

Several inconsistencies arose between the appearance of the masseter muscle in the cadaver cryosections and the MR images. First, only four inscriptions were observed in the coronal MR images compared to the five which were described earlier in the cryosectioned cadaver muscle. These observations, while consistent with the work of Ebert (1939) were not consistent with the internal organization of the muscle reported by Schumacher (1961). As the tendon planes appeared to extend only partially into the muscle mass, adjacent muscle layers appeared continuous with one another nearer the centre of the muscle. This ambiguity might be due to either signal averaging effects, or to receiver coil insensitivity. Of the two, the former explanation is the more likely since the MR signal was detectable from as deep as the medial pterygoid muscle. Signal averaging of these delicate strands of tissue through the 5mm MR slice might cause them to appear merged with signal from closely adjacent surrounding tissues. In the superficial part of the muscle, it appeared that sehnenspiegel 2 and 3 were fused within the muscle mass to produce our tendon plane (II).

Second, a low-intensity signal representing tendinous inscriptions was not seen in all areas of the muscle as might be expected from the cryosectioned cadaver muscle. The thickest, and most lateral inscription, sehnenspiegel 1 (Schumacher, 1961a) appeared in the coronal cryosections separating the muscle body medially from glandular tissue lateral to it. On the corresponding MR image, this same arrangement was expected. However, while muscle and glandular tissue were observed, a thick, low-intensity signal band representing tendon was not seen. One reason could be due to the excitation characteristics of the RF coil, and the image display parameters which were chosen. Superficial tissues experience more excitation than deeper ones. Consequently, they are magnetized to a greater extent. The effect of the strong signal from the surrounding adipose tissue might have saturated the lower intensity tendon signal producing a "bloom" effect around it, thereby masking it from view. Another explanation could be that adipose tissue infiltration into adjacent regions of the tendon and the signal averaging process might have given rise to the strong MR signal which was observed. If this is the case, then one might expect to find the presence of connective tissue fascia in addition to tendon in these areas. This same appearance was seen on both the medial and lateral sides of the deep masseter muscle, where high intensity signal clefts are seen. This observation might suggest that the original assumptions made by Schumacher (1961a) regarding the nature of these tissues (fascial and/or tendinous), and their role during function (Gans and Bock, 1965) might require re-evaluation. Anatomically, these voids were not observed in the cryosections and without histological sectioning in these regions, it is difficult to estimate the extent of adipose tissue associated with the tendon.

If these inscriptions are fascial rather than tendinous in nature, then our current views on internal masseter muscle function might need to be altered. The appearance of these regions on the coronal MR images would suggest that the human masseter muscle is made up of two distinct parts, one superficial and one deep. Between them is an inscription of fascial tissue which suggests independent, rather than coordinated function of the two

parts. The organization of tendon in the superficial part of the muscle suggests it is capable of developing lines of action consistent with other multipennate muscles. In the deep part of the masseter, the tendon organization would suggest the existence of an independent unipennate system.

5.1.4 Three-Dimensional Muscle Reconstruction and Tendon Plane Generation

Three-dimensional morphological reconstruction from two-dimensional planar image sets has been used by others to estimate whole jaw muscle orientations and angulations in humans (Hannam and Wood, 1989; Koolstra et al, 1990). Koolstra et al (1990) reported that the differentiation of muscle and fascial tissue was better in coronal images and this contributed to easier reconstructions. Their reconstructions however, consisted of stacked two-dimensional profiles of tissue sections traced from MR images. They also ascertained that poor muscle reconstructions could result from minor head movements during image acquisition, slice thickness or tracing errors. Minor head movements from breathing and swallowing are a concern during the image acquisition process, since these may distort, or blur tissue boundaries making the next step, tissue contour tracing, more difficult. For these studies, slice thickness was only a concern near the origins and insertions of the muscles where the amount of tissue for signal averaging was less. Slice thickness is of greater concern for more sophisticated image processing methods which employ algorithms to produce a surface skin between sectional, planar contours. Two approaches have been used in the past to model these surfaces. The first involves representing the surface as a mosaic of flat, usually triangular, polygon tiles. The second, a more complicated technique, involves the use of more sophisticated curve patches to generate the surface. For these, as Sinclair et al (1990) have pointed out, the problem of approximating surfaces between successive slice contours is greatly reduced when their separation approaches zero. This is particularly important when adjacent contours are irregular or dissimilar in shape. To overcome this problem, contiguous 5mm MR images were acquired. However, even with these thinner sections, surface generation between adjacent tissue contours continued to be

of concern.

The disposition and amount of tendon associated with the human masseter muscle complicated the problem of irregularly-shaped muscle contours. In coronal cross section, these appeared as spicules of tendon extending into the muscle mass. As muscle was the only tissue traced, regions on the MR images where tendon was present, but not traced, appeared sharp with numerous concavities. This proved a demanding task for the software. Not only did it have to produce a surface skin between highly irregular muscle contours, it had to do so without generating artifactual ripples, or twist, into the surface. This problem was alleviated somewhat by the filtering process which "smoothed" the tissue contours before they were transferred into the surface rendering routine.

Depending on the size and complexity of a particular tissue contour, it could be represented by as many as several hundred data points. Each contour was then reduced to 50 equally spaced data points because of the memory limitations imposed by the computer system. The magnitude of this alteration was of course greater for larger tissue sections, where one data point in 5 or 6 was used to describe a section of each tissue contour, than for the smaller ones, where one data point in 2 or 3 was used. The result of this process was smoother tissue contours which were particularly obvious around areas with finger-like tissue projections. The 50 point tissue contour was then transferred to the surface rendering routine which reorganized the points, placing more nodes around these complex regions, and fewer nodes around the less complex areas.

The surface topography of the reconstructed masseter muscle was found to be irregular and somewhat curvilinear. In coronal cross-section, these sections were also slightly ellipsoid in shape. These features of the muscle constrained alignment of planar quadrilaterals to the muscle surface so that putative tendon planes were fitted to the most uniformly planar regions of the muscle surface. In some areas where the surface was

irregular, the fitted planes either intersected the surface or ran slightly superficial to it.

5.1.5 Bite Force Transducer and Calibration

The 1/2ins diameter FSR^{TM} which was employed was easily adapted for our purposes. The manufacturer suggests that the output voltage of the device is repeatable to ±2% for the same FSR^{TM}, and ±15% for similar units over 100g. They also suggest preloading of the device before use. In our experience, device preloading of at least 1000g was necessary to minimize drift of the FSR^{TM} output voltage in use. Below this preload limit, a non-linear response between FSR^{TM} output voltage and force was found.

As well, the response of the FSR^{TM} was highly sensitive to the angle of the load point. This is again consistent with the product information which suggests the use of a bearing point orthogonal to the surface of the FSR^{TM}. In addition, the response of the device varied with the location of the bearing point, which was not mentioned in the product syllabus. Using a steel dome which covered the entire sensing surface of the FSR^{TM} and constraining bite force orthogonally to the dome apex, easily reproducible results could be obtained.

5.1.6 Occlusal Stop Fabrication

The occlusal stop design incorporated shallow indentations on its occlusal surface to prevent eccentric movements of the jaw during exercise. These helped to provide some positive stops for the opposing dentition. While attempts were made to constrain the direction of the clenching effort vertically by employing as flat an acrylic surface as possible for the opposing maxillary teeth, the subjects reported some difficulty maintaining this effort without sliding off the stop. Discrepancies in the direction of the clench may have produced some of the variations observed, particularly between left- and right-sided clenching.

The thickness of the occlusal stop was designed to match that of the force

transducer. By its very nature, the stops introduced the variable of vertical dimension into the study. Manns et al (1977) studied the relationship between bite force and jaw opening and found them to be linearly related from 0.5mm to 20mm of increased vertical dimension, at 80% maximal masseter muscle activity. In order to isolate first molar contacts, some increase in vertical dimension was required. In a later study, Manns et al (1981) demonstrated a 14% decrease in integrated EMG activity in whole masseter muscles with 4mm to 5mm increases in vertical dimension. Whether this increase alters the pattern of regional activity in the masseter muscle is, however, unknown.

5.1.7 Exercise Protocol

As Christensen (1979, 1980a, 1981) has shown, subjects cannot normally maintain a maximal, or near-maximal isometric clench for greater than approximately 108sec. As 128 signal acquisitions lasting approximately 4min were necessary to generate acceptable MR spectra during exercise, it would be impossible for subjects to maintain constant muscle activity at this level for the time period required. Therefore, a protocol was developed in which subjects were asked to clench maximally for 1sec and then rest for 1sec. This was done to the rhythm of an external auditory signal which could be heard from within the spectrometer. While the subjects complied with these instructions, all reported post-exercise pain in both muscles shortly after finishing the last exercise and this persisted up to two days.

5.1.8 Magnetic Resonance Spectroscopy

Until recently, the biopsy technique provided the only means for monitoring muscle metabolism directly, and while these studies contributed significantly to our knowledge of muscle function during isometric and dynamic exercise, they were simply too invasive. ^{31}P MR spectroscopy is ideally suited for non-invasive examinations of metabolic activity over time. *In-vivo* applications of ^{31}P MR spectroscopy were pioneered by Moon and Richards in 1973. The abundance of phosphate *in vivo* is comparatively small compared to that of the

proton, and as a result, phosphorous MR experiments were, for many years, confined to the high magnetic fields which could be generated in small bore animal magnets. The introduction of whole body, high field, superconducting magnets, revolutionized human ^{31}P MR spectroscopy experiments, *in vivo*.

As of yet, absolute metabolite concentrations cannot be measured because of uncertainties of coil receiver volume and position (Taylor et al, 1983). Therefore, the concentrations of P_i and PCr have been reported as normalized units. Phosphate from ATP is not included in the total phosphate equation because the chemical shift of the ATP peaks suggest that it is predominately complexed to Mg^{2+} (Gadian and Radda, 1981). Free ADP concentration is also not considered significant, since much of this is bound to actin, and perhaps other proteins as well (Meyer et al, 1982). Discrepancies have been found between *in-vitro* determinations of P_i concentration by ^{31}P MR spectroscopy and traditional chemical assays (Ackerman et al, 1980). These have been attributed to the possibility that during the freezing and extraction phases of the chemical analysis, artifactual hydrolysis of PCr occurs, contributing higher P_i concentrations. Another possibility is that a significant proportion of P_i exists in a bound state in the mitochondria, which is undetectable by ^{31}P MR.

The determination of intracellular pH is a valuable tool in ^{31}P MR spectroscopy. The accuracy of the method relies on the ability to construct appropriate titration curves of the chemical shift of a metabolite versus pH in solutions designed to mimic the intracellular cytoplasmic environment (Burt et al, 1976). Roos and Boron (1981) considered the ^{31}P MR determination of intracellular pH to be superior to conventional methods because of its high precision.

5.2 Discussion of the Data

5.2.1 Cephalometry

While the bony elements of the skull serve to anchor the muscles, tendons and

ligaments which power and suspend the mandible, there is a surprisingly poor correlation between conventional lateral cephalometric landmarks and whole muscle angulation (Hannam and Wood, 1989). In our subject group, cephalometric radiography revealed some disparate skeletal forms. For example, subject 4 possessed a relatively short ramus (4.3cm) and a low facial height (5.4cm). In the orthogonal coronal view, this subject had narrow bizygomatic (11.0cm) and bigonial (9.2cm) widths and a narrow "masseteric width" of 0.9cm. The craniofacial dimensions of subject 5 were very different from this. Subject 5 had a long ramal length (5.6cm) and tall lower face (8.1cm). Because bizygomatic and bigonial widths were equally large (13.0cm and 11.2cm, respectively), the "masseteric width" was equal to that found for the much smaller faced subject 4. However, unless the masseter muscle has uniform medial-lateral width from origin to insertion, "masseteric width" cannot provide an accurate estimate of the true muscle width. Measuring the breadth of each muscle compartment transversely (approximating each as an angulated ellipse) was believed to provide a more accurate estimate of the functional width of muscle tissue displacing the tendon planes. These measurements produced surprisingly similar results for the intermediate and deep compartments, but not for the superficial compartment. As expected, subject 5 demonstrated the largest superficial masseter of the group. Unexpectedly, subject 1, who had the largest masseteric width (1.5cm) had the smallest superficial masseter and subject 3 who had a large superficial masseter, did not have a very great "masseteric width". It seems that bizygomatic and bigonial width are of little value for estimating the breadth of functional muscle compartments.

5.2.2 Tendon Plane Angle Estimation

Individually, some subjects demonstrated slight deviations in tendon plane angulation on either side of the parasagittal plane. In the coronal view, the extramuscular tendon planes (I) and (IV) showed the greatest mean angulation away from this plane. The intramuscular tendon planes (II and III) were more vertically oriented. In the axial view, variations in individual planar angles between subjects was much greater. Because the

same three-dimensional vector was used to define the fitted plane in both the coronal and axial views, these variations cannot be attributed to independent errors introduced by separate views of the same structure. The angulation of plane (I) was medially angled anteriorly, no doubt following the angulation of the zygomatic arch. Plane (II) was angled in the opposite direction, and plane (III) was nearly parallel to plane (I). Plane (IV) was angled away from the midsagittal plane, probably conforming to the surface of the lateral face of the mandibular ramus. The angulations of these planes appeared to follow the relative orientations of the zygomatic arch and lateral surface of the mandibular ramus. The disposition of these hard tissue surfaces clearly has an important bearing on tendon plane angulation, and presumably creates greater variations in the axial than in the coronal view.

An analysis of bipennate muscle structure, such as the one described by Gans and Bock (1965) suggests that muscle fibres are anchored about a central tendon. When these fibres are activated, tension is developed in the muscle fibres at an angle α, the pennation angle, relative to the axis of the tendon plane. The net result is displacement of the tendon plane and shortening of the muscle along the same axis. This arrangement makes three assumptions about internal muscle structure and function. First, the inter-plane distances from the central tendon to adjacent ones must be equal if the angle of pennation is equivalent on either side of the tendon. Second, the pennation angle must be equal for adjacent fibre sets on either side of a central tendon if displacement is to occur along the tendon axis; and third, both muscle fibre sets must contract synergistically and develop the same tension. This important relationship between α and tendon translation prompted Gans and de Vree (1987) to suggest that the former should be measured relative to the plane of tendon translation.

The unique three-dimensional orientation of each tendon plane found in this study suggests that the angle of pennation may be different according to the viewing plane used and is determined by the relative positions and angulations of the ramal surface and

zygomatic arch in three dimensions. Hence, in a muscle like the masseter, α should be more correctly expressed as a three-dimensional angle relative to the plane of a given tendon. The different planar orientations of tendons which were observed suggest that fibre orientations between planes may not result in equal pennation angles at their proximal and distal ends, and support the notion of differential shortening within the muscle, whether or not activation occurs evenly during contraction. In function however, it is likely that these structural relationships change, and do so in a manner which can only be determined by serial imaging in different jaw positions.

5.2.3 Quantification of ^{31}P Magnetic Resonance Spectra

Mean resting P_i/PCr ratios have been reported variously as 0.10 in human flexor digitorum profundus muscle (extracted from Taylor et al, 1983), 0.12±0.01 in the human wrist flexor muscles (McCully et al, 1988), and 0.14±0.03 in human gastrocnemius muscle (McCully et al, 1988). McCully et al (1989) found no difference in the mean resting P_i/PCr ratio of trained versus untrained individuals. In an attempt to relate muscle fibre type to this parameter, Meyer et al (1985) studied slow- and fast-twitch muscles in the cat hind limb. They demonstrated mean resting P_i/PCr ratios of 0.089 in cat biceps muscle which is composed of greater than 75% fast-twitch, glycolytic fibres, and 0.568 in cat soleus, which is greater than 92% slow-twitch, oxidative fibres. They suggested that differences in these ratios between different muscles and within regions of the same muscle might prove useful for routine non-invasive estimation of fibre type in humans. The human masseter muscle, which predominantly consists of slow-twitch, oxidative type I fibres (Eriksson and Thornell, 1983), displayed mean resting P_i/PCr ratios comparable to the cat soleus in the anterior superficial (0.40±0.13) and intermediate (0.42±0.13) regions. The deep part of the muscle displayed higher mean P_i/PCr ratio (0.70±0.17) at rest, possibly reflecting the slightly higher proportion of type I fibres in this region (Eriksson and Thornell, 1983). The mean normalized P_i concentration ($[P_i]$) at rest has been found to be 0.08 in cat biceps and 0.36 in cat soleus muscles (Meyer et al, 1988). Our mean $[P_i]$ of 0.29±0.06, 0.29±0.05 and 0.41±0.06 at rest,

are again, comparable to the cat soleus muscle. The mean percentage of type I fibres in the wrist flexors, in contrast, is 44.5% for human flexor digitorum brevis and 47.3% for human flexor digitorum profundus; 57.4% in human first dorsal interosseous and 43.5% to 50.8% in human gastrocnemius muscles (Johnson et al, 1973) which may partially explain the smaller P_i/PCr ratios observed in these muscles.

During steady state dynamic exercise, McCully et al (1989) reported a mean increase in the P_i/PCr ratio to 1.36±0.14 and to 1.32±0.13 for trained and untrained individuals respectively, in the human wrist flexor muscles. Recent evidence by Cady and Newham (1989) for the human first dorsal interosseous muscle performing isometric exercise, demonstrated that there was no significant difference between mean metabolite levels between 50% and 100% of maximal exercise (as evidenced by ^{31}P MR spectroscopy). Our subjects were able to maintain greater than 81.6% of their maximum bite force during the exercise paradigm outlined earlier, and demonstrated mean increases to between 1.09±0.47 and 1.70±0.89 for left molar clenching, and between 1.23±0.77 and 1.54±0.60 for right molar clenching, indicating an increase in PCr utilization during these exercises. The mean [P_i] increased to between 0.50±0.13 and 0.58±0.11 for left molar clenching, and between 0.49±0.16 and 0.59±0.10 for right molar clenching which is consistent with the trend demonstrated by Challis et al (1988) in exercising rat hind limb muscle.

The mean metabolic activity in the deep part of the right masseter muscle during left molar clenching was found to be greater than the mean activity for right molar clenching. Although this result was not statistically significant, the observation is contrary to the findings of Greenfield and Wyke (1956) and Belser and Hannam (1986) who found the exact opposite for ipsilateral molar clenching and chewing using electromyography. Individually, four of the six subjects displayed higher P_i/PCr ratios during left sided molar clenching than right. This discrepancy might be accounted for by differences in craniofacial morphology or muscle activation strategies between the subjects, but the result remains an enigma.

The mean resting pH in human skeletal muscle derived from ^{31}P MR spectra has been reported to be 7.03±0.03 in human flexor digitorum superficialis (Taylor et al, 1983), 7.02±0.02 and 6.98±0.02 in trained and untrained human wrist flexor muscles (McCully et al, 1989) and 7.10±0.03 in human first dorsal interosseous muscle (Cady and Newham, 1989) during steady state exercise. Meyer et al (1985) found a mean resting pH of 7.18 in both fast- and slow-twitch muscles of the cat hind limb. Our mean resting regional values of 7.14±0.08, 7.11±0.06 and 7.17±0.03 are consistent with these results. During dynamic exercise, Taylor et al (1983) reported a mean decrease in pH to 6.4 and 6.8 in the human finger and wrist flexors, respectively. McCully et al (1989) reported a mean decrease to 6.87±0.089 in untrained subjects. Cady and Newham (1989) reported a mean pH drop in human first dorsal interosseous muscle during isometric exercise to 6.60±0.11 and 6.61±0.09 at 50% and 100% maximum voluntary contraction. During isometric exercise, the mean pH of our subjects decreased to between 6.99±0.08 and 7.03±0.05, with the greatest individual decrease to 6.82. The relatively small drop in pH values seen in our experiments might be attributed to the "fitness" of the jaw muscles, since McCully et al (1989) reported that trained subjects in ramp exercise tests had a significantly higher ($p<0.05$) mean end-exercise pH (6.91±0.04) compared with untrained subjects (6.72±0.07).

During exercise, aerobic oxidative phosphorylation is the primary mode of ATP synthesis in type I skeletal muscle fibres. During active muscle contraction Taylor et al (1983) observed that anaerobic metabolism, and hence lactic acid formation, is only significantly activated when PCr has decreased to approximately 40% of its resting value. This would correspond to an equivalent $[P_i]$ of approximately 0.28 for the superficial and intermediate parts, and 0.23 for the deep parts of the masseter muscle. During prolonged, heavy exercise, ATP is consumed at a much higher rate than can be replenished by both the cytosolic creatine kinase and through oxidative metabolism. The biosynthesis of ATP through anaerobic (glycolytic) pathways then becomes an important mechanism of energy regeneration. This is particularly true for type II fibres. However, as the rate of ATP

utilization approaches the maximum rate of ATP biosynthesis by oxidative phosphorylation, anaerobic glycolysis begins to take over an increasing proportion of the metabolic burden. Classically, the explanation for this has been that part of the muscle is O_2 deficient and energy production must be supplemented by glycolysis. Recent work by Connett et al (1984, 1985) suggested that anaerobic glycolysis, even at low work intensities is critical for the production and maintenance of substrate concentrations for oxidative ATP production. Together, the marked increase in $[P_i]$, the decrease in PCr and the relative constancy of the intracellular pH in our data during isometric exercise suggests that most of the metabolic activity is confined to oxidative muscle fibres, however, there might be some participation from anaerobic fibres, given the slight decrease in intracellular pH.

Cohen et al (1989) examined only one region of the masseter muscle using ^{31}P MR spectroscopy and demonstrated that subjects diagnosed as myofascial pain dysfunction syndrome patients displayed a less evident phosphate ratio signature and that they were unable to recover as quickly to a rest "signature" value compared to asymptomatic subjects. Our results point out the necessity for examining the human masseter muscle in parts rather than as a whole, since differences in resting metabolite levels are different, particularly between the deep part of the muscle and the other regions.

5.3 Future Directions

In the first of these studies, anatomical compartmentalization was elucidated in the human masseter muscle by tendinous septa to demonstrate the existence of an anatomical substrate for functional heterogeneity. Histologic sectioning of the adult muscle might usefully distinguish tendon from fascia and adipose tissue. As well, thinner MRI sections available on more modern MR units will provide higher resolution anatomical data of the muscle. In function, it is likely that these structural relationships change. Therefore, to better understand the internal mechanics of the muscle in different jaw positions, serial imaging and three-dimensional graphical reconstruction in different jaw positions would be

an asset.

The metabolic profiles of these putative muscle compartments were elucidated in a separate set of functional studies. Although three of the experimental subjects participated in both studies, it was not possible to correlate metabolic profiles with anatomic regions within these same muscles. Recently, new methods of spatial localization has been developed for this purpose (Ordidge et al, 1986; Blackledge et al, 1987). These hybrid techniques allow ^{1}H MR image-guided ^{31}P MR signal acquisition three dimensionally however, spectral S/N can be compromised without a significant increase in the number of signal acquisitions. In the future, these methods should be rapidly developed, since Jeneson et al (1990) recently acknowledged the importance of anatomical compartmentalization in ^{31}P MR studies of the human finger flexor muscles.

The temporal onset and recovery of metabolic activity is an important measure for determining muscle fitness. This has already been quantified in some limb muscles. In the jaws, this would necessitate higher S/N spectra, since it would be advantageous to acquire ^{31}P MR spectra every 1 to 2 minutes. The recent introduction of 4.0T whole body MR systems would be a great advantage here. The relationship between metabolic activity, particularly during recovery, and intramuscular capillary perfusion would also be an interesting field to explore, since the role of the vasculature in metabolite clearance is not known, and must be an important factor during exercise and recovery.

Finally, the efficacy of the ^{31}P MR technique as a diagnostic tool for evaluating jaw muscle pathosis should also be investigated. One preliminary study by Cohen et al (1989) has already suggested that metabolic recovery is slower in subjects with diagnosed muscle pathosis.

CHAPTER 6

Summary

The recent introduction of magnetic resonance imaging into clinical radiology has enhanced medical diagnosis in numerous tissue and organ systems throughout the body. In dental radiology, the growth of MR as a diagnostic tool has regrettably not progressed beyond investigations of disk position in the temporomandibular articulation. Therefore, the initial impetus of this work was the application of the ^{1}H MR imaging technique to the study skeletal muscle and tendon organization in the human masseter muscle. Employing a pulse sequence originally devised for imaging the ligaments and soft tissues of the knee (King et al, 1986) a technique was developed for obtaining thin, 5mm sections through the human masseter muscle. A novel algorithm (Sinclair et al, 1989) allowed three-dimensional reconstruction of the digitized MR images, and visualization of the solid object. The same software also permitted positioning of putative tendon planes represented by planar quadrilaterals tangent to the reconstructed muscle according to the criteria of Ebert (1939) and Schumacher (1961a). The unique three-dimensional angulation of each tendon plane and the variation of their positions within the muscle suggests that heterogeneity of function in different muscle regions may have an anatomical basis in the organization of the muscle.

Anatomical compartmentalization of the human masseter muscle elucidated by MR imaging provided the basis for a metabolic study of muscle contraction. Although mean resting muscle pH was similar in the anterior superficial, posterior intermediate and deep parts of the muscle, significant differences in mean resting metabolic activity was found in the deep masseter compared to the superficial and intermediate regions. During intermittent, isometric exercise, metabolic activity increased in all parts of the muscle without a difference between left- and right-sided clenching. An accompanying decrease in mean muscle pH was also observed in all muscle regions. The magnitude of this decrease suggests a generally high "fitness level" for the human masseter muscle.

Future studies could readily combine the MR imaging and ^{31}P MR spectroscopy techniques to study the structure and functional behaviour of the human masseter muscle. As well, the results of the ^{31}P MR study are significant enough to warrant additional investigation of muscles in subjects with craniomandibular dysfunction.

CHAPTER 7

Bibliography

Ackerman J.J.H., Grove T.H., Wong G.G., Gadian D.G., and Radda G.K. (1980). Mapping of metabolites in whole animals by ^{31}P NMR using surface coils. *Nature* 283, 167-170.

Ahlborg G. and Felig P. (1982). Lactate and Glucose Exchange across the Forearm, Legs and Splanchnic Bed during and after Prolonged Leg Exercise. *Clin. Invest.* 69, 45-54.

Axel L. (1984). Relaxation Times and NMR Signals. *Mag. Res. Imag.* 2, 121-130.

Bailey I.A., Williams S.R., Radda G.K. and Gadian D.G. (1981). Activity of phosphorylase in total global ischaemia in the rat heart. *Biochem. J.* 196, 171-178.

Bárány M. (1967). ATPase Activity of Myosin Correlated with Speed of Muscle Shortening. *J. Gen. Physiol.* 50 (No 6, Part 2), 197-216.

Baron P. and Debussy T. (1979). A Biomechanical Functional Analysis of the Masticatory Muscles in Man. *Archs. Oral Biol.* 24, 547-553.

Becht G. (1954). Comparative biologic-anatomical researches on mastication in some mammals, I & II. *Proc. K. ned. Akad. Wet.* (Series C) 56, 508-527.

Belser U.C. and Hannam A.G. (1986). The contribution of the deep fibers of the masseter muscle to selected tooth-clenching and chewing tasks. *J. Prosthet. Dent.* 56, 629-635.

Benninghoff A. and Ebinger (1946). Über die Mechanik des normalen und den Umbau des atrophischen Muskels. *Ärztl. Wschr.* 1, 251.

Benninghoff A. and Rollhäuser H. (1952). Zur inneen Mechanik des gefiederten Muskels. *Pflügers Arch. ges. Physiol.* 254, 527-548.

Bergström J., Hermansen L., Hultman E. and Saltin B. (1971). Energy rich phosphagens in dynamic and static work. *Adv. Exp. Med. Biol.* 11, 341-355.

Blackledge M.J., Styles P. and Radda G.K. (1987). Rotating-Frame Depth Selection and Its Application to the Study of Human Organs. *J. Mag. Res.* 71, 246-258.

Bloch F., Hansen W.W. and Packard M. (1946). Nuclear induction. *Phys. Rev.* 69, 127.

Bonde-Petersen F. and Christensen L.V. (1973). Blood flow in human temporal muscle during tooth grinding and clenching as measured by ^{133}Xe clearance. *Scand. J. Dent. Res.* 81, 272-275.

Bottomley P.A., Foster T.H., Argersinger R.E. and Pfeifer L.M. (1984). A review of normal hydrogen NMR relaxation times and relaxation mechanisms from 1-100MHz: dependence on tissue type, temperature, species excision and age. *Med. Phys.* 11, 425-448.

Brown T. (1965). Morphology of the Australian Skull, In Australian Aboriginal Studies, No. 49. Australian Institute of Aboriginal Studies, Canberra.

Burke R.E., Levine D.N., Tsaris P. and Zajac F.E. (1973). Physiological types and histochemical profiles in motor units of the cat gastrocnemius. *J. Physiol.* 234, 723-748.

Burt C.T., Glonek T. and Bárány M. (1976). Analysis of Phosphate Metabolites, the Intracellular pH, and the State of Adenosine Triphosphate in Intact Muscle by Phosphorous Nuclear Magnetic Resonance. *J. Biol. Chem.* 251, 2584-2591.

Busby S.J.W., Gadian D.G., Radda G.K., Richards R.E. and Seeley P.J. (1978). Phosphorous nuclear magnetic resonance studies of compartmentalization in muscle. *Biochem. J.* 170, 103-114.

Bydder G.M., Curati W.L., Gadian D.G., Hall A.S., Harman R.R., Butsen P.R., Gilderdale D.J. and Young I.R. (1985). Use of Closely Coupled Receiver Coils in MR Imaging: Practical Aspects. *J. Comput. Assist. Tomog.* 9, 987-996.

Cady E.B. and Newham D.J. (1989). Metabolism and Fatigue in Human Skeletal Muscle During Isometric Contractions at Three Intensities. Proceedings of the 8th Annual Meeting of the Society of Magnetic Resonance in Medicine, Amsterdam, p. 543.

Challiss R.A.J., Brackledge M.J. and Radda G.K. (1988). Spatial heterogeneity of metabolism in skeletal muscle in vivo studied by ^{31}P-NMR spectroscopy. *Am. J. Physiol.* 254 (Cell Physiol. 23), C417-422.

Chance B., Leigh J.S. Jr., Clark B.J., Maris J., Kent J., Nioka S. and Smith D. (1985). Control of oxidative metabolism and oxygen delivery in human skeletal muscle: A steady-state analysis of the work/energy cost transfer function. *Proc. Natl. Acad. Sci. U.S.A.* 82, 8384-8388.

Chance B., Younkin D.P., Kelley R., Bank W.J., Berkowitz H.D., Argov Z., Donlon E., Boden B., McCully K., Buist N.M.R. and Kennaway N. (1986). Magnetic resonance spectroscopy of normal and diseased muscles. *Am. J. Med. Gen.* 25, 659-679.

Christensen L.V. (1967). Facial pain from the masticatory system induced by experimental bruxism. *Tandlaegebladet* 71, 1171-1181.

Christensen L.V. (1970). Facial pain from experimental tooth clenching. *Tandlaegebladet* 74, 175-182.

Christensen L.V. (1971). Facial pain and internal pressure of masseter muscle in experimental bruxism in man. *Archs. Oral Biol.* 16, 1021-1031.

Christensen L.V. (1976). Facial pain in negative and positive work of human jaw muscles. *Scand. J. Dent. Res.* 84, 327-332.

Christensen L.V. (1978). Mast cells in masseter muscle in experimental bruxism. *J. Oral Rehabil.* 5, 23-27.

Christensen L.V. (1979). Some subjective experimental parameters in experimental tooth clenching in man. *J. Oral Rehabil.* 6, 119-136.

Christensen L.V. (1980a). Some electromyographic parameters of experimental tooth clenching in adult human subjects. *J. Oral. Rehabil.* 7, 139-146.

Christensen L.V. (1980b). Some electromyographic parameters of experimental tooth clenching in children. *J. Oral Rehabil.* 7, 379-386.

Christensen L.V. (1981). Progressive jaw muscle fatigue of experimental tooth clenching in man. *J. Oral Rehabil.* 8, 413-420.

Christensen L.V. and Mohamed S.E. (1984). Contractile activity of the masseter muscle in experimental clenching and grinding of the teeth. *J. Oral Rehabil.* 11, 191-199.

Christensen L.V. (1985). Pains from the jaw muscles in children and adults. In Orthodontics: State of the Art, Essence of the Science. Ed. E Graber. The CV Mosby Co., St. Louis, MI., pp. 28-47.

Christiansen E.L., Thompson J.R., Hasso A.N., Hinshaw D.B. Jr., Moore R.J., Roberts D. and Kopp S. (1987). CT Number Characteristics of Malpositioned TMJ Menisci, Diagnosis with CT Number Highlighting (Blinkmode). *Invest. Radiol.* 22, 315-322.

Cohen S.G., Lenkinsky R., Zavatsky A. and Roberts D. (1989). Magnetic Resonance Spectroscopic Analysis of Masticatory Muscles. *J. Dent. Res.* 68, 391.

Connett R.J. (1987). Glycolytic regulation during an aerobic rest-to-work transition in dog gracilis muscle. *J. Appl. Physiol.* 63, 2366-2374.

Connett R.J., Gayeski T.E.J. and Honig C.H. (1984). Lactate accumulation in fully aerobic working dog gracilis muscle. *Am. J. Physiol.* 246, H120-H128.

Connett R.J., Gayeski T.E.J. and Honig C.H. (1985). Energy sources in fully aerobic rest-work transitions: a new role for glycolysis. *Am. J. Physiol. 248,* H922-H929.

Connett R.J., Honig C.R., Gayeski T.E.J. and Brooks G.A. (1990). Defining hypoxia: a systems view of V_{O2}, glycolysis, energetics and intracellular P_{O2}. *J. Appl. Physiol.* 68, 833-842.

Cox P.J. and Rothwell P.S. (1984). Serum creatine kinase studies in mandibular pain dysfunction. *J. Oral Rehabil.* 11, 45-52.

Damadian R. (1971). Tumor detection by nuclear magnetic resonance. *Science* 171, 1151-1153.

Dawson M.J., Gadian D.G. and Wilkie D.R. (1977). Contraction and recovery of living muscles studied by ^{31}P nuclear magnetic resonance. *J. Physiol.* 267, 703-735.

Dubowitz V. and Brooke M.H. (1973). Muscle biopsy - a modern approach. WB Saunders, London, pp.34-102.

DuBrul E.L. (1980). Sicher's Oral Anatomy, 7th Ed. The CV Mosby Co, St. Louis, MI, pp. 147-149.

Ebert H. (1939). Morphologische und Funktionelle analyse des Musculus masseter. *Z. anat. EntwGesch.* 109, 790-802.

Edström L. and Kugelberg E. (1968). Histochemical composition, distribution of fibres and fatiguability of single motor units. *J. Neurol. Neurosurg. Psychiat.* 31, 424-433.

Eriksson P.-O. and Thornell L.-E. (1983). Histochemical and Morphological Muscle-Fibre Characteristics of the Human Masseter, the Medial Pterygoid and the Temporal Muscles. *Archs. Oral Biol.* 28, 781-795.

Gadian D.G. and Radda G.K. (1981) N.M.R. studies of tissue metabolism. *Annu. Rev. Biochem.* 50, 69-84.

Gadian D.G., Radda G.K., Richards R.E. and Seeley P.J. (1979). ^{31}P in living tissue: the road from a promising to an important tool in biology. In Biological Applications of Magnetic Resonance. Ed. R.G. Shulman. Academic Press, New York, N.Y., pp. 463-533.

Gans C. and Bock W.J. (1965). The functional significance of muscle architecture - a theoretical analysis. *Ergebn. Anat. Entwickl.* 38, 115-142.

Gans C. and de Vree F. (1987). Functional Bases of Fiber Length and Angulation in Muscle. *J. Morphol.* 192, 63-85.

Gaspard M., Laison F. and Mailland M. (1973). Organization architecturale et texture du muscle masseter chez les Primates et l'Homme. *J. Biol. Buccale* 1, 7-20.

George P. and Rutman R.J. (1960). The "high energy phosphate bond" concept. *Prog. Biophys. Biophys. Chem.* 10, 2-53.

Greenfield B.E. and Wyke B.D. (1956). Electromyographic Studies of Some of the Muscles of Mastication, I. Temporal and masseter activity in various jaw movements in normal subjects. *Brit. Dent. J.* 100, 129-143.

Häggmark T. and Thorstensson A. (1979). Fibre types in human abdominal muscles. *Acta. Physiol. Scand.* 107, 319-325.

Hands L.J., Bore P.J., Galloway G., Morris P.J. and Radda G.K. (1986). Muscle metabolism in patients with peripheral vascular disease investigated by ^{31}P nuclear magnetic resonance spectroscopy. *Clin. Sci.* 71, 283-290.

Hannam A.G. and Wood W.W. (1989). Relationships Between the Size and Spatial Morphology of Human Masseter and Medial Pterygoid Muscles, the Craniofacial Skeleton and Jaw Biomechanics. *Am. J. Phys. Anthropol.* 80, 429-445.

Harms S.E., Wilk R.M., Wolford L.M., Chiles D.G. and Milam S.B. (1985). The temporomandibular joint: magnetic resonance imaging using surface coils. *Radiology* 157, 133-136.

Heinze W. (1972). Strukturanalytische Untersuchungen an den Muskeln der Vorderund Hintergliedmasse des Schweines sowie Erörterung einiger allgemeinmyologrischer Probleme, 3. *Ant. Anz.* 130, 251-270.

Helpern J.A., Kao W., Gross B., Kensora T.G. and Welch K.M.A. (1989). Interleaved ^{31}P NMR with Transcutaneous Nerve Stimulation (TNS): A Method of Monitoring Compliance-Independant Skeletal Muscle Metabolic Response to Exercise. *Mag. Res. Med.* 10, 50-56.

Herfkens R.J. and Johnson G.A. (1985). Magnetic Resonance Imaging at High-Strength Magnetic Fields. In Magnetic Resonance Annual 1985. Ed. H.Y. Kressel. Raven Press, New York, N.Y., pp. 197-215.

Herring S.W. (1975). Adaptations for gape in the hippopotamus and its relatives. *Forma et Functio* 8:85-100.

Herring S.W., Grimm A.F. and Grimm B.R. (1979). Functional Heterogeneity in a Multipinnate Muscle. *Am. J. Anat.* 154, 563-576.

Herring S.W. and Scapino R.P. (1973). Physiology of feeding in miniature pigs. *J. Morph.* 141, 427-460.

Herring S.W., Wineski L.E. and Anapol F.C. (1989). Neural Organization of the Masseter Muscle in the Pig. *J. Comp. Neurol.* 280, 563-576.

Hiiemae K. (1967). Masticatory function in the mammals. *J. Dent. Res.* 46, 883-893.

Hiiemae K. and Houston W.J.B. (1971). The structure and function of the jaw muscles in the rat (*Rattus norvegicus* L.) I. Their anatomy and internal architecture. *Zool. J. Linn. Soc.* 50, 75-99.

Hiiemae K. (1971). The structure and function of the jaw muscles in the rat (*Rattus norvegicus* L.) II. Their fibre type and composition. *Zool. J. Linn. Soc.* 50, 101-109.

Hoult D.I., Busby S.J.W., Gadian D.G., Radda G.K., Richards R.E. and Seeley P.J. (1974). Observation of tissue metabolites using ^{31}P nuclear magnetic resonance. *Nature* 252, 285-287.

Hultman E., Sjöholm H., Sahlin K. and Edström L. (1981). Glycolytic and oxidative energy metabolism and contraction characteristics of intact human muscle. In Human muscle fatigue: physiological mechanisms. Eds. Porter R. and Whelan J. Pitman Medical (Ciba Foundation), London, pp. 19-39.

Issekutz B., Jr. (1984). Effect of β-adrenergic blockade on lactate turnover in exercising dogs. *J. Appl. Physiol.* 57, 1754-1982.

Jansson E., Sjödin B. and Tesch P. (1978). Changes in muscle fibre type distribution in man after physical training - A sign of fibre type transformation? *Acta Physiol. Scand.* 104, 235-237.

Jeneson J.A.L., Wesseling M.W., de Boer R.W. and Amelink A.G. (1989). Peak-splitting of inorganic phosphate during exercise: anatomy or physiology? A MRI-guided ^{31}P MRS study of human forearm muscle. Proceedings of the 8th Annual Meeting of the Society of Magnetic Resonance in Medicine, Amsterdam, p. 1030.

Jeneson J.A.L., Taylor J.S., Vigneron D.B., Willard T.S., Carvajal L., Nelson S.J., Murphy-Boesch J. and Brown T.R. (1990) ^{1}H MR Imaging of Anatomical Compartments within the Finger Flexor Muscles of the Human Forearm. *Mag. Res. Med.* 15, 491-496.

Johnson M.A., Polgar J., Weightman D. and Appleton D. (1973). Data on the distribution of fibre types in thirty-six human muscles. An autopsy study. *J. Neurol. Sci.* 18, 111-129.

Katzberg R.W., Schenck J., Roberts D., Tallents R., Manzione J.V., Hart H., Foster T., Wayne W.S. and Bessette R.W. (1985). Magnetic resonance imaging of the temporomandibular joint meniscus. *Oral Surg.* 59, 332-335.

Katzberg R.W., Bessette R.W., Tallents R.H., Plewes D.B., Manzione J.V., Schenck J.F., Foster T.H. and Hart H.R. (1986). MR imaging with surface coil. *Radiology* 158, 183-189.

King C.L., Henkelman M., Poon P.Y. and Rubenstein J. (1984) MR Imaging of the Normal Knee. *J. Comput. Assist. Tomog.* 8, 1147-1154.

Koolstra J.H., van Eijden T.M.G.J., van Spronsen P.H., Weijs W.A. and Valk J. (1990). Computer-assisted estimation of lines of action of human masticatory muscles constructed *in vivo* by means of magnetic resonance imaging of parallel sections. *Archs. Oral Biol.* 35, 549-556.

Kugelberg E. (1976). Adaptive transformation of rat soleus motor units during growth - Histochemistry and contraction speed. *J. Neurol. Sci.* 27, 269-289.

Kumar A., Welti D. and Ernst R. (1975). NMR Fourier Zeugmatography. *J. Mag. Res.* 18, 69-78.

Kushmerick M.J. (1983). Energetics of muscle contraction. In Handbook of Physiology. Eds. Peachey L.D., Adrian R.H. and Geiger S.K. Waverly Press, Baltimore, MD., pp. 189-236.

Lauterbur P.C. (1973). Image formation by induced local interactions: examples employing NMR. *Nature* 242, 190-191.

Lowe A.A. (1980). Correlations between orofacial muscle activity and craniofacial morphology in a sample of normal and anterior open-bite subjects. *Am. J. Orthodont.* 78, 89-98.

Manns A. and Spreng M. (1977) EMG Amplitude and Frequency at Different Muscular Elongations Under Constant Masticatory Force or EMG Activity. *Acta physiol. latinoam.* 27, 259-271.

Manns A., Miralles R. and Guerrero F. (1981) The changes in electrical activity of the postural muscles of the mandible upon varying the vertical dimension. *J. Prosthet. Dent.* 45, 438-445.

McCully K.K., Argov Z., Boden B.P., Brown R.L., Bank W.J. and Chance B. (1988). Detection of muscle injury in humans with 31-P magnetic resonance spectroscopy. *Muscle & Nerve* 11, 212-216.

McCully K.K., Boden B.P., Tuchler M., Fountain M.R. and Chance B. (1989). Wrist flexor muscles of elite rowers measured with magnetic resonance spectroscopy. *J. App. Physiol.* 67, 926-932.

McMillan A.S. and Hannam A.G. (1989). Motor Unit Territory in the Human Masseter Muscle. *J. Dent. Res.* 68, 951.

McMinn R.M., Hutchings R.T. and Logan B.M. (1981). Head and Neck Anatomy. Year Book Medical Publishers Inc., Chicago IL., pp. 114-115.

Meyer R.A., Kushmerick M.J. and Brown T.R. (1982). Application of ^{31}P-NMR spectroscopy to the study of striated muscle metabolism. *Am. J. Physiol.* 242 (Cell Physiol 11), C1-C11.

Meyer R.A., Brown T.R. and Kushmerick M.J. (1985). Phosphorous nuclear magnetic resonance of fast- and slow-twitch muscle. *Am. J. Physiol.* 248, C279-C287.

Monteiro A.A. and Kopp S. (1988). Estimation of blood flow by ^{133}Xe clearance in human masseter muscle during rest, endurance of isometric contraction, and recovery. *Archs. Oral Biol.* 33, 561-565.

Moon R.B. and Richards J.H. (1973). Determination of intracellular pH by ^{31}P magnetic resonance. *J. Biol. Chem.* 248, 7276-7278.

Newham D.J., McPhail G., Mills K.R. and Edwards R.H.T. (1983). Ultrastructural changes after concentric and eccentric contractions of human muscle. *J. Neurol. Sci.* 61, 109-122.

Newham D.J., Jones D.A. and Clarkson P.M. (1987). Repeated high-force eccentric exercise: effects on muscle pain and damage. *J. Appl. Physiol.* 63, 1381-1386.

Newsholme E.A. (1970). Theoretical and Experimental Considerations on the Control of Glycolysis in Muscle. In Essays in Cell Metabolism. Eds. Bartley W., Kornberg H.L. and Quayle J.R. Wiley-Interscience, London, pp.189-224.

Newsholme E.A. and Start (1973). Regulation in Metabolism. John Wiley & Sons, London, pp.88-145.

Ordidge R.J., Connelly A. and Lohman J.A.B. (1986) Image-Selected *in Vivo* Spectroscopy (ISIS). A New Technique for Spatially Selective NMR Spectroscopy. *J. Mag. Res.* 66, 283-294.

özand P. and Narahara H.T. (1964). Regulation of Glycolysis in Muscle, III. Influence of insulin, epinephrine and contraction on phosphofructokinase activity in frog skeletal muscle. *J. Biol. Chem.* 239, 3146-3152.

Park J.H., Brown R.L., Park C.R., McCully K., Cohn M., Haselgrove J. and Chance B. (1987). Functional pools of oxidative and glycolytic fibers in human muscle observed by ^{31}P magnetic resonance spectroscopy during exercise. *Proc. Nat. Acad. Sci. U.S.A.* 84, 8976-8980.

Purcell E.R., Torrey H.C. and Pound R.V. (1946). Resonance absorption by nuclear magnetic moments in a solid. *Phys. Rev.* 69, 37-38.

Ramaiah A. (1976). Regulation of glycolysis in skeletal muscle. *Life Sci.* 19, 455-466.

Rasmussen O.C., Bonde-Petersen F., Christensen L.V. and Møller E. (1977). Blood flow in human mandibular elevators at rest and during controlled biting. *Archs. Oral Biol.* 22, 539-543.

Rauschning W., Bergström K. and Pech P. (1983). Correlative Craniospinal Anatomy Studies by Computed Tomography and Cryomicrotomy. *J. Comp. Assist. Tomog.* 7, 9-13.

Ringqvist M. (1974). Fiber types in human masticatory muscles - Relation to function. *Scand. J. Dent. Res.* 82, 333-355.

Ringqvist M., Ringqvist I., Eriksson P.-O. and Thornell L.-E. (1982). Histochemical Fibre-Type Profile in the Human Masseter Muscle. *J. Neurol. Sci.* 53, 273-282.

Roberts D., Schenck J.F., Joseph P., Foster T., Hart H., Pettigrew J., Kundel H.L., Edelstein W. and Haber B. (1985). Temporomandibular joint: magnetic resonance imaging. *Radiology* 147, 139-148.

Romer A.S. (1939). The vertebrate body, 1st Ed. WB Saunders & Co., Philadelphia, PA.

Roos A. and Boron W.F. (1981) Intracellular pH. *Physiol. Rev.* 61, 296-434.

Saltin B. (1973). Skelettmuskelfiberns egenskaper och funktion. *Forskn. Prakt.* 5, 77-81.

Schellhas K.P. (1989). MR Imaging of Muscles of Mastication. *A.J.N.R.* 10, 829-837.

Schiaffino S. (1974). Histochemical Enzyme Profile of the Masseter Muscle in Different Mammalian Species. *Anat. Rec.* 180, 53-62.

Schumacher, G.H. (1961a). Die Kaumuskulatur der Menschen. In Funktionelle Morphologie der Kaumuskulatur. Veb Gustav Fischer Verlag, Jena, pp. 13-53.

Schumacher, G.H. (1961b). Die Kaumuskulatur der Rodentia. In Funktionelle Morphologie der Kaumuskulatur. Veb Gustav Fischer Verlag, Jena, pp. 189-209.

Schumacher, G.H. (1961c). Die Kaumuskulatur der Carnivoren. In Funktionelle Morphologie der Kaumuskulatur. Veb Gustav Fischer Verlag, Jena, pp. 99-151.

Schumacher, G.H. (1961d). Die Kaumuskulatur der Artiodactyla. In Funktionelle Morphologie der Kaumuskulatur. Veb Gustav Fischer Verlag, Jena, pp. 152-188.

Seltzer S.E. and Wang A.M. (1987). Modern imaging of the masseter muscle: normal anatomy and pathosis on CT and MRI. *Oral Surg., Oral Med., Oral Pathol.* 63, 622-629.

Shupe R.J., Mohamed S.E., Christensen L.V., Finger I.M. and Weinberg R. (1984). Effects of occlusal guidance on jaw muscle activity. *J. Prosthet. Dent.* 51, 811-818.

Sinclair B., Hannam A.G., Lowe A.A. and Wood W.W. (1989). Complex Contour Organization for Surface Reconstruction. *Comput. & Graphics* 13, 311-319.

Suzuki A. (1977). A Comparative Histochemical Study of the Masseter of the Cattle, Sheep, Swine, Dog, Guinea Pig, and Rat. *Histochemistry* 51, 121-131.

Stålberg E. and Eriksson P.-O. (1987). A Scanning Electromyographic Study of the Topography of Human Masseter Single Motor Units. *Archs. Oral Biol.* 32, 793-797.

Stewart W.A. (1986). Quantitative NMR imaging and its applications *in vivo*. M.Sc. Thesis, the University of British Columbia, Vancouver.

Tanuma K. (1984). Changes with Advance of Age of the Human Maxillomandibularis, Zygomaticomandibularis and Superficial Temporalis. *Okajimas Folia Anat. Jpn.* 61, 1-14.

Taylor A. (1976). Fibre Types in the Muscles of Mastication. In Mastication. Eds. Anderson D.J. and Matthews B. Wright and Sons Ltd., Dorchestor, pp. 16-24.

Taylor D.J., Bore P.J., Styles P., Gadian D.G. and Radda G.K. (1983). Bioenergetics of Intact Human Muscle, A ^{31}P Nuclear Magnetic Resonance Study. *Mol. Biol. Med.* 1, 77-94.

Tonndorf M.L., Sasaki K. and Hannam A.G. (1989). Single-Wire Recording of Regional Activity in the Human Masseter Muscle. *Brain Res. Bull.* 23, 155-159.

Unger J.M. (1985). The Oral Cavity and Tongue: Magnetic Resonance Imaging. *Radiology* 155, 151-153.

van Spronsen P.H., Valk J., Weijs W.A. and Prahl-Andersen B. (1987). Analysis of masticatory muscle orientation in adults by means of MRI. *Acta anat.* 130, 96-97.

Wallace T.W., Evaskus D.S. and Laskin D.M. (1979). Serum isoenzyme changes in experimental bruxism. *J. Dent. Res.* 58, 26.

Weijs W.A. (1973). Morphology of the muscles of mastication in the albino rat, *Rattus Norvegicus* (Berkenhout, 1769). *Acta morph. neerl. scand.* 11, 321-340.

Weijs W.A. and Dantuma R. (1975). Electromyography and Mechanics of Mastication in the Albino Rat. *J. Morph.* 146, 1-345.

Weijs W.A. and Hillen B. (1986). Correlations between the cross-sectional area of the jaw muscles and craniofacial size and shape. *Am. J. Phys. Anthropol.* 70, 423-430.

Westesson P.-L., Katzberg R.W. and Tallents R.H. (1987). CT and MR of the temporomandiublar joints: comparison with autopsy specimens. *A.J.R.* 148, 1165-1171.

Young I.R., Burl M. and Bydder G.M. (1986) Comparative Efficiency of Different Pulse Sequences in MR Imaging. *J. Comput. Assist. Tomog.* 10, 271-286.